Peer review information: *Nature Communications* thanks Ayako Nakamura-Ishizu and the other, anonymous, reviewer(s) for their contribution to the peer review of this work.

Niche Derived Netrin-1 Regulates Hematopoietic Stem Cell Dormancy via its Receptor Neogenin-1

Simon Renders[1,2,3], Arthur Flohr Svendsen[4,16], Jasper Panten[1,2,5,16], Nicolas Rama[6,16], Maria Maryanovich[7,8], Pia Sommerkamp[1,2,5], Luisa Ladel[1,2], Anna Rita Redavid[6], Benjamin Gibert[6], Seka Lazare[4], Benjamin Ducarouge[6], Katharina Schönberger[9], Andreas Narr[1,2,5], Manon Tourbez[4], Bertien Dethmers-Ausema[4], Erik Zwart[4], Agnes Hotz-Wagenblatt[10], Dachuan Zhang[7,8], Claudia Korn[11,12], Petra Zeisberger[1,2], Adriana Przybylla[1,2], Markus Sohn[1,2], Simon Mendez-Ferrer[11,12], Mathias Heikenwälder[13], Maik Brune[14], Daniel Klimmeck[1,2], Leonid Bystrykh[4], Paul S. Frenette[7,8], Patrick Mehlen[6], Gerald de Haan[4], Nina Cabezas-Wallscheid[9,17], Andreas Trumpp[1,2,15,17]

[1] Division of Stem Cells and Cancer, German Cancer Research Center (DKFZ) and DKFZ-ZMBH Alliance, 69120 Heidelberg, Germany

[2] Heidelberg Institute for Stem Cell Technology and Experimental Medicine (HI-STEM gGmbH), 69120 Heidelberg, Germany

[3] Department of Internal Medicine V, Heidelberg University Hospital, Heidelberg, Germany.

[4] Laboratory of Ageing Biology and Stem Cells, European Research Institute for the Biology of Ageing, University Medical Center Groningen, University of Groningen, Groningen, The Netherlands

[5] Faculty of Biosciences, Heidelberg University, Heidelberg, Germany

[6] Apoptosis, Cancer and Development Laboratory, Equipe labellisée "La Ligue," LabEx DEVweCAN, Institut Convergence Rabelais, Centre de Recherche en Cancérologie de Lyon, INSERM U1052-CNRS UMR5286, Université de Lyon1, Centre Léon Bérard, 69008 Lyon, France

[7] Ruth L. and David S. Gottesman Institute for Stem Cell and Regenerative Medicine Research, Albert Einstein College of Medicine, Bronx, NY, USA.

[8] Department of Cell Biology, and Department of Medicine Albert Einstein College of Medicine, Bronx, NY, USA

[9] Max Planck Institute of Immunobiology and Epigenetics, 79108 Freiburg, Germany

[10] Core Facility Omics IT and Data Management, German Cancer Research Center (DKFZ), Heidelberg, Germany

[11] Wellcome Trust/ MRC Cambridge Stem Cell Institute & Department of Haematology, University of Cambridge, Cambridge, CB2 0AH, UK.

[12] NHS Blood and Transplant, Cambridge, CB2 0PT, UK

[13] Division of Chronic Inflammation and Cancer, German Cancer Research Center Heidelberg (DKFZ), Heidelberg, Germany

[14] Department of Internal Medicine I and Clinical Chemistry, Heidelberg University Hospital, Heidelberg, Germany.

[15] German Cancer Consortium (DKTK), 69120 Heidelberg, Germany

[16] These authors contributed equally

[17] These authors jointly supervised this work

Correspondence to a.trumpp@dkfz.de or cabezas@ie-freiburg.mpg.de

Abstract

Haematopoietic stem cells (HSCs) are characterized by their self-renewal potential associated to dormancy. Here we identify the cell surface receptor Neogenin-1 as specifically expressed in dormant HSCs. Loss of Neogenin-1 initially leads to increased HSC expansion but subsequently to loss of self-renewal and premature exhaustion *in vivo*. Its ligand Netrin-1 induces *Egr1* expression and maintains quiescence and function of cultured HSCs in a Neo1 dependent manner. Produced by arteriolar endothelial and periarteriolar stromal cells, conditional Netrin-1 deletion in the bone marrow niche reduces HSC numbers, quiescence and self-renewal, while overexpression increases quiescence *in vivo*. Ageing associated bone marrow remodelling leads to the decline of Netrin-1 expression in niches and a compensatory but reversible upregulation of Neogenin-1 on HSCs. Our study suggests that niche produced Netrin-1 preserves HSC quiescence and self-renewal via Neogenin-1 function. Decline of Netrin-1 production during ageing leads to the gradual decrease of Neo1 mediated HSC self-renewal.

INTRODUCTION

Haematopoietic stem cells (HSCs) are highly quiescent and give rise to cycling multipotent progenitors (MPPs), which are in turn responsible for maintaining steady state hematopoiesis[1-5]. Upon transplantation, HSCs harbour multi-lineage and serial long-term engraftment potential [6-9]. The CD34 negative HSC compartment is heterogeneous and consists of both dormant HSCs (dHSCs) and active HSCs (aHSCs) with dHSCs showing superior serial engraftment potential[10, 11]. dHSCs can be identified *via* label retention approaches[10-13] or by employing *Gprc5c-GFP* reporter mice[11]. All dHSCs reside in a transcriptionally and metabolically rather inactive state and rest in the G_0 cell cycle phase.

Upon ageing the number of immunophenotypic HSCs increases, but their capability to self-renewal diminishes and a myeloid differentiation bias emerges[14-19]. Various HSC intrinsic hallmarks of ageing, such as the disruption of cellular polarity, and epigenetic instability have been identified[20-22]. Concomitantly, it has become clear that the bone marrow (BM) microenvironment undergoes remodelling upon ageing and contributes to functional decline of HSCs[23-25]. Still, the crosstalk between extrinsic niche derived and HSC intrinsic factors mediating stem cell maintenance and quiescence, particularly in the context of ageing, remains elusive[26, 27]. Based on this, we hypothesize that changes in interactions maintaining quiescence in young bone marrow may contribute to the functional decline of HSCs.

A number of cell surface receptors, activated by niche-derived ligands such as THPO-MPL, DARC-CD82 or Histamin-H2R, have been described to directly modulate HSC behaviour[28-31]. Interestingly, some of these, including CXCR4-CXCL12 and SCF-cKIT, also seem to play a key role during neural development[32, 33]. Neogenin-1 (Neo1), a cell surface receptor first identified as a regulator of axon guidance, has been implicated in a wide variety of functions ranging from cell migration and survival to angiogenesis[34]. Its role has recently also been studied in the innate and adaptive immune systems[35-37]. It shares almost 50% amino acid homology with Deleted in Colorectal Cancer (DCC)[38, 39]. The extracellular domain of Neo1 has been described to bind members of both the “Repulsive Guidance Molecule” (RGMa-c) and Netrin (Ntn) families[34, 39]. Neo1 can modulate cytoskeletal activities and can function as a co-receptor for BMPs[40, 41]. However, the functional role of Neo1 or its ligands such as Ntn1 in HSC biology remain uncertain[1, 42]. Here, we identify Ntn1-Neo1 signalling as an important regulator of HSC quiescence.

RESULTS

Neo1 is specifically expressed in the most quiescent HSCs

Neo1 expression in HSCs has previously been reported by us and others [1, 42-44]. To further characterize *Neo1* expression within the hematopoietic stem and progenitor cell (HSPC) compartment, we isolated various HSPC populations (**Figure 1a and S1a**) and found *Neo1* to be exclusively expressed in HSCs (**Figure 1b**). This HSC-specific expression pattern of NEO1 was also apparent at the protein level (**Figure 1c and S1b**). NEO1 levels in HSCs were heterogenous as about 20% of HSCs expressed particularly high levels on the surface (**Figure 1c**). Next, we studied whether this subset of NEO1 high-expressing HSCs correspond to dormant HSCs (dHSCs) by conducting label retaining assays using *SCL-tTA;H2B-GFP* mice[10] (**Figure S1c**). After 150 days of doxycycline chase, we found *Neo1* transcripts and protein to be expressed at higher levels in dHSCs compared to aHSCs and MPP1s, suggesting that *Neo1* is associated with dormancy (**Figure 1d-e**). As expected, dHSCs specifically expressed the dHSC marker *Gprc5c*[11] (**Figure S1d)**. To independently validate increased *Neo1* expression in dHSCs, we employed *Gprc5c-GFP* reporter mice and isolated dormant GFP^{pos} and active GFP^{neg} HSCs (**Figure S1e**). In agreement, we found higher Neo1 RNA and protein levels in Gprc5c-GFP^{pos} versus Gprc5c-GFP^{neg} HSCs (**Figure S1f-g**). As HSCs are a highly quiescent population during steady state, we next addressed whether *Neo1* levels not only rapidly diminished during hematopoietic differentiation, but also upon HSC activation. Therefore, we treated mice with either poly-I:C (pIC) mimicking viral, or LPS mimicking bacterial infection[45, 46]. HSCs showed a robust, reversible loss of *Neo1* expression in response to either stimulus (**Figure 1f-g**). Collectively, these data strongly link *Neo1* expression to dormancy in HSCs.

Neo1-mutant mice reveal a competitive advantage upon transplantation

Considering the HSC-specific expression pattern of *Neo1*, we set out to study the function of Neo1 in the hematopoietic system. Unfortunately, in our hands, no commercial antibody allowed the robust and reproducible isolation of viable $Neo1^{+}$ cells by flow cytometry when using *Neo1*-mutant cells as controls[42]. Thus, we employed a *Neo1* gene-trapped mouse model to genetically address the functional role of Neo1 in HSC biology ($Neo1^{gt/gt}$)[38, 47, 48]. Although *Neo1* expression in the BM of mutant mice was diminished by >90% (**Figure 2a**), the hematopoietic

compartment did not exhibit altered HSPC or mature cell frequencies in 5 to 6-week-old animals (**Figure S1h**). To analyse Neo1-deficient hematopoiesis, we performed reconstitution analysis with BM cells derived from 5-6-week-old *Neo1*-mutant animals (**Figure 2b**). Firstly, we non-competitively transplanted total BM derived from *Neo1*-mutant or control littermates (CD45.2) into CD45.1 recipients and assessed HSC numbers four months after primary or secondary transplantation (**Figure 2c**). We observed that the frequency of HSCs, while similar at 4 months after transplantation, increased in *Neo1*-mutant chimeras upon secondary transplantation. To further investigate this expansion of HSCs, we performed competitive transplantations of *Neo1*-mutant or control BM cells (**Figure 2d**). We found that *Neo1*-mutant BM cells showed a competitive advantage compared to control counterparts as evident by peripheral blood leukocyte contribution in secondary recipients and in BM HSC contribution in primary and secondary transplantations (**Figure 2e-f)**. As HSC frequencies in both transplantation assays increased over time, we also investigated primary chimeras eight months after transplantation and again found an increase in HSC numbers in *Neo1*-mutant chimeras (**Figure 2g-h**). We observed no difference in HSC homing (**Figure 2i-j**), suggesting that self-renewal and output of *Neo1*-mutant HSCs is altered.

Aged *Neo1*-mutant HSCs display features of premature exhaustion

Next, we addressed whether the HSC expansion observed in *Neo1*-mutant chimeras would lead to malignant transformation or HSC exhaustion over time (**Figure 3a**). Interestingly, 15 months after the generation of primary chimeras, the initial expansion of the *Neo1*-mutant HSC pool reverted and both HSC and MPP1 frequencies decreased (**Figure 3b**). When we compared absolute blood counts in aged *Neo1*-mutant chimeras to controls, we found reduced absolute lymphocyte and neutrophil counts as well as reduced haemoglobin levels indicative of hematopoietic malfunction (**Figure 3c**). As expected, chimeras displayed increased myeloid differentiation upon ageing, and this effect was exacerbated in in *Neo1*-mutant chimeras over time (**Figure 3d**). To address whether this decline in mature cell output was caused by an HSC defect, we re-transplanted one hundred CD45.2^{+} HSCs derived from either aged *Neo1*-mutant or control chimeras (**Figure 3e**). Four months after transplantation, *Neo1*-mutant HSCs had generated significantly less progeny then controls (**Figure 3f**). To validate functional exhaustion, we re-

transplanted BM of aged chimeras into secondary and tertiary recipients (**Figure 3g**). In these mice, aged *Neo1*-mutant BM exhibited a pronounced failure to engraft and depletion of HSCs and all MPP populations was observed, suggesting that the original *Neo1*-mutant HSCs from the aged chimeras had a decreased self-renewal potential (**Figure 3h-i**). Meanwhile, we observed no increase in malignancies arising in *Neo1*-mutant chimeras. Next, we analysed cell cycle behaviour of *Neo1*-mutant HSCs. We found less HSCs residing in G0 phase in 4-5 weeks old *Neo1*-mutant mice compared to their control littermates (**Figure S1i**). This decrease in G0-HSCs was also apparent in full chimeras both 4 and 8 months after transplantation (**Figure 3j-k and S1j**) and *Neo1*-mutant HSCs expressed higher levels of the cell cycle activation marker CDK6. Additionally, increased incorporation of BrdU above the expected injection induced activation was observed in *Neo1*-mutant HSCs (**Figure 3l-m and S1k**). Altogether, *Neo1*-mutant HSCs harbour diminished long-term repopulation potential, associated with a loss of quiescence and increased proliferation.

Molecular signatures of activation and HSC dysfunction are enriched in *Neo1*-mutant HSCs

To understand the molecular basis for the disruption of long-term self-renewal caused by loss of Neo1, we performed RNA-seq analysis of $Neo1^{gt/gt}$ and Wt CD45.2^{+} HSCs 4 months (expanding *Neo1*-mutant HSCs) and 15 months (exhausted *Neo1*-mutant HSCs) after transplantation (**Figure 4a and S2a**). Principal component analysis showed the main mode of transcriptional variation to be attributable to age. The molecular consequences of mutant *Neo1* was recapitulated by PC-2 and the difference increased upon ageing (**Figure 4a and S2b)**. As expected, *Neo1* expression itself was diminished in *Neo1*-mutant HSCs, but interestingly strongly upregulated in aged compared to young Wt HSCs (**Figure S2c**). Analysis of shared functional differences between young and old *Neo1*-mutant HSCs compared to controls using Gene Set Enrichment Analysis (GSEA), we revealed cell cycle associated gene sets like *Hallmark(HM)_Mitotic_Spindle* and *HM_G2M_Checkpoint to be* enriched in *Neo1*-mutants (**Figure 4b)** validating the functional data. This pattern of increased activation in *Neo1*-mutant HSCs was also observed employing HSC-specific cell cycle signatures[49] (**Figure 4b**). In line with these data, the signature for *aHSCs* was enriched in *Neo1*-mutant HSCs, in turn the signature for *dHSCs* was

enriched in Wt HSCs[11] (**Figure 4b**). Reflecting the observed functional deficits of *Neo1*-mutant HSCs, the *MoIO*[50] signature associated with superior HSC function was overrepresented in Wt HSCs, while the *NoMO* signature[50], enriching for less quiescent, functionally inferior HSCs was enriched in *Neo1*-mutant HSCs (**Figure 4b**). Analysis of differentially expressed genes (DEGs) identified genes associated with differentiation such as *Itga2b* and *Gata1*[50-52] as well as cell cycle regulators such as *Cdk6*[53] (**Figure 4c, S2f**) or *Mki67* (**Figure S2d**) to be upregulated in *Neo1*-mutant HSCs. In contrast, genes known to regulate HSC self-renewal or quiescence, such as *Egr1*[54, 55], *Zfp36*[56] and c-*Fos*[57] were downregulated (**Figure 4c, S2f**). Interestingly, Cdk6 has been shown to supress *Egr1* expression during HSC activation, which was suggested to promote HSC quiescence based on genetic data and thus is a likely downstream target of Neo1[54]. No other Ntn1 receptors were differentially expressed (**Figure S2e**). Therefore, the molecular data support the functional findings by revealing footprints of both loss of quiescence and diminished expression of HSC self-renewal related genes in *Neo1*-mutant HSCs. Additionally, we found that HSC ageing signatures[20] were enriched in *Neo1*-mutant HSCs reflecting the observed functional decline (**Figure 4d**). In line, *Klf6,* which has been proposed to maintain features of young HSCs in human, was downregulated in *Neo1*-mutant HSCs[58] (**Figure 4e, S2f**). Finally, we report gene sets associated with NF-κB signalling, as well as signalling of the NEO1 ligand Netrin-1 (Ntn1) to be depleted in *Neo1*-mutant HSCs, suggesting that these signalling pathways may be downstream of NEO1 activation (**Figure 4f**).

Interestingly, when we tested enrichment for the *Reactome_Netrin-1_Signalling* gene set on RNA-seq data of a recent study of HSPC[1], it was enriched in HSCs compared to all MPP populations, suggesting that Ntn-1 signalling is physiological active in homeostatic HSCs (**Figure S2g**). In summary, we discover molecular features of both loss of quiescence and loss of self-renewal in *Neo*1-mutant HSCs, paralleling functional results.

NTN1 maintains HSC engraftment potential and quiescence *via* NEO1 signalling

Next, we assessed whether the NEO1 ligands NTN1, RGM-a and RGM-b alone or in combination with their co-ligand BMP-2 were able to affect HSC behaviour. Because neither *RGM*s and *Ntn1* nor additional Ntn1 receptors were expressed in HSCs

(**Figure S2h**)[1], we sorted and cultured HSCs in the presence of NTN1, RGM-A and RGM-B with or without BMP-2 (**Figure 5a**). To assess active NEO1 signalling, we monitored *Egr1* expression, which was down-regulated in *Neo1*-mutant HSCs (**Figure 5b)**. After 48 hours of stimulation, only NTN1, but none of the other ligands, induced expression of *Egr1* (**Figure 5b**). This induction was absent in *Neo1*-mutant HSCs (**Figure 5b**). In addition, we detected a Neo1 dependent decrease in G2-S-M and an increase in G0 phase HSCs as well as diminished CDK6 protein levels (**Figure 5c-d**), paralleling the data from *Neo1*-mutant HSCs *in vivo* (**Figure 4c and 4g**). We further confirmed induction of quiescence by NTN1 with HSCs isolated from *FUCCI*[59] and *c-Myc-GFP* mice[60] reporter mice (**Figure S2i-j**). Gene sets associated with NF-κB signalling were downregulated in *Neo1*-mutant HSCs. Since NF-κB is essential for HSC maintenance and known to protect HSCs from premature differentiation upon stress[61], we hypothesized that NTN1 may induce NF-κB signalling. To test this hypothesis, we isolated HSCs from *p65-GFP* mice, cultured them +/- NTN1 or +/- the p65 nuclear translocation inhibitor JSH-23 (**Figure 5e**). We observed increased nuclear p65 levels upon NTN1 treatment, which was blocked by JSH-23 (**Figure 5e**), suggesting that NTN1 maintains the canonical NF-κB pathway. We next assessed whether *in vitro* NTN1 stimulation translates into improved HSC engraftment *in vivo*. For this purpose, we stimulated 500 HSCs derived from either CD45.2 or CD45.1/2 mice with or without Ntn1 for 48h, mixed treated with untreated congenically distinct HSCs and transplanted them into lethally irradiated recipients (**Figure 5f**). Four months after transplantation, we found increased engraftment of HSCs cultured with NTN1 in the BM, independent of genotype (**Figure 5g**). This showed that *ex vivo* treatment with NTN1 robustly improved the *in vivo* function of cultured HSCs. This effect of NTN1 was dependent on the presence of NEO1 since it was absent in *Neo1*-mutant HSCs (**Figure S2k**). Collectively, these data suggest that the NTN1-NEO1 axis preserves NF-κB activity, quiescence and *in vivo* function of cultured HSCs.

Conditional Ntn1 deletion depletes HSCs and leads to activation and differentiation *in vivo*

Next, we addressed the role of Ntn1 in hematopoiesis *in vivo*. Mice homozygous for a Ntn1 null allele ($Ntn1^{ß\text{-}geo/ß\text{-}geo}$) die perinatally due to defects in cerebral development[62] and heterozygous mice display no hematopoietic phenotype (**Figure**

S3a). Therefore, we generated *CAGGS:Cre^{ERT2}*; *Ntn1$^{flox/flox}$* mice[63,64], which allows tamoxifen (Tam) inducible ubiquitous deletion of *Ntn1* (**Figure S3h)**. We induced deletion of *Ntn1* at 6 weeks after birth (*Ntn1$^{\Delta CAGGSCre/\Delta CAGGSCre}$*) and analysed mice 8 weeks later (**Figure 6a**). *Ntn1* deletion caused an increase in the relative frequencies of myeloid cells, especially neutrophils in both peripheral blood and BM (**Figure S3b-d**). Strikingly, the frequency of HSCs in *Ntn1$^{\Delta CAGGSCre/\Delta CAGGSCre}$* BM, was significantly reduced, while simultaneously the frequency of both MPP2 and MPP3/4 cells expanded (**Figure 6b-c and S3e-f**). In response to the induced *Ntn1* deletion, HSCs entered a more proliferative, less quiescent state, represented by an increase of HSCs in G2-S-M and a reduction in G0 (**Figure 6d**). After *Ntn1* deletion, HSCs also expressed reduced levels of *Egr1,* while expression of *Cdk6*, as well as the differentiation associated genes *Gata1* and *Itga2b* increased (**Figure 6e**). Finally, *Neo1* expression was upregulated in *Ntn1$^{\Delta CAGGSCre/\Delta CAGGSCre}$* HSCs, suggesting a compensatory upregulation in response to the absence of its ligand (**Figure 6e**).

The observed reduced numbers of HSCs were even more pronounced at 5 months post *Ntn1* deletion, suggesting a progressive loss of HSCs after *Ntn1* deletion (**Figure 6f and S3g/i**). To test whether increased levels of NTN1 could alter HSC behaviour *in vivo*, we generated *CAGGS:Cre^{ERT2}; LSL-Rosa26-Ntn1 mice* (*Ntn1-OE*) and induced Cre expression in 6 week-old animals, leading to a 30-fold increase of *Ntn1* levels in BM endothelial cells after 5 months (**Figure S3h**). While we found no difference in HSPC frequencies (**Figure S3j**), quiescent G0-HSCs increased, suggesting that *Ntn1* overexpression in the BM microenvironment leads to increased HSC quiescence *in vivo* (**Figure 6g and S3k)**. Additionally, the frequency of cycling HSCs 5 months after *Ntn1* deletion was significantly increased, reproducing the 2 month time-point (**Figure 6d,g and S3k**). In summary, Ntn1 mediates HSC quiescence not only in culture, but also *in vivo* and loss of *Ntn1* activates and progressively depletes quiescent, functional HSCs.

Conditional Ntn1 deletion impairs HSC function

To study, whether the Netrin-1 mediated increase (*Ntn1-OE*) or reduction in HSC quiescence and frequency (*Ntn1* deletion) is associated with functional consequences, we competitively transplanted total bone marrow of *Ntn1-OE,* *Ntn1$^{\Delta CAGGSCre/\Delta CAGGSCre}$* or control (*CAGGS-Cre^{ERT2}*) mice five months after Tamoxifen induction (**Figure 6h**). Upon *Ntn1-OE* we neither observed any

differences in peripheral blood leukocytes, nor in HSC frequencies four months after transplantation (**Figure 6i-k**). In contrast, *Ntn1* deletion led to a reduced contribution of CD45.2+ donor cells to peripheral blood leukocytes (**Figure 6i-j**) accompanied with a strong reduction of HSC numbers four months after transplantation (**Figure 6k**). Next, we addressed the engraftment potential of 200 purified HSCs (LSK, $CD150^+$, $CD48^-$, $CD34^-$) isolated either from a microenvironment, in which Ntn1 was deleted for five months (*Ntn1*$^{\Delta CAGGSCre/\Delta CAGGSCre}$) or expressed on normal levels (**Figure 6l**). Two months post-transplantation, the HSC frequency was significantly reduced compared to control HSC, which have developed in a Ntn1 proficient environment (**Figure 6m**). These data show that HSCs derived from a *Ntn1* deficient BM become functionally impaired and this self-renewal defect is not reversed by transplanting them back into a Ntn1 proficient recipient microenvironment.

Ntn1 expressed by arterioles maintains HSCs

We next investigated which niche cells express *Ntn1*. By screening published datasets, we found that *Ntn1* is expressed at low levels in sinusoidal (SEC: $CD45^-$, $CD31^+$, Sca-1^{medium}, $Pdpn^+$) and at higher levels in arteriolar endothelial cells (AEC: $CD45^-$, $CD31^+$, Sca-1^{high}, $Pdpn^-$)[65]. Additionally, *Ntn1* expression has been reported in periarteriolar smooth muscle cells[66]. To examine *Ntn1* expression within the bone marrow niche, we isolated AECs, SECs, $CD45^+$ hematopoietic and RFP^+ cells derived from *Sma-RFP* reporter mice marking smooth muscle cells (SMC)[67] (**Figure S4a-b**). While we found no expression in $CD45^+$ hematopoietic cells, we detected the highest *Ntn1* levels in AECs and smooth muscle cells (**Figure 7a**). To investigate whether periarteriolar smooth muscle derived Ntn1 regulates HSCs, we generated *Sma-Cre*^{ERT2}*; Ntn1*$^{flox/flox}$ mice*,* injected adult mice with tamoxifen and studied HSCs 8 weeks after Cre induction. In line with depletion of HSCs upon global Ntn1 deletion, we detected a decrease in HSCs in *Ntn1*$^{\Delta SmaCre/\Delta SmaCre}$ animals compared to controls (**Figure 7b**). This reduction was however not as strong as we observed upon global *Ntn1* deletion using CAGGS-Cre (**Fig. 6**), suggesting additional Ntn1 sources like AECs. As BM arterioles deteriorate upon ageing, leading to the loss of HSC maintaining stem cell factor (SCF)[23, 24], we isolated SECs and AECs from young and old Wt mice and found diminished *Ntn1* expression specifically in old AECs (**Figure 7c**). When we investigated *Neo1* in aged HSCs, we found expression was still restricted to HSCs, but levels were significantly increased (**Figure S4c**), in line with

our RNA-seq data from aged Wt chimeras (**Figure S2d**). To further confirm this, we performed RNA-seq of young and old LSK-SLAM cells. We found *membrane-associated* processes and *receptors* to be upregulated upon ageing (**Figure S4d**). Specifically, Neo1 expression increased robustly on RNA and protein level in old HSCs (**Figure 7d-e**). Several studies have previously compared transcriptional profiles of young versus old HSCs (using different marker combinations). However, the studies showed a wide variety of DEGs with little consistency (**Figure S4e**). To identify consistently changed DEGs upon HSC ageing, we added 12 previously published transcriptome datasets of aged HSCs to our own study and performed a meta-analysis (**Figure S4e**). In these 13 datasets, not a single DEG was shared among 10 or more studies, again highlighting the heterogeneity. Nevertheless, 13 genes were consistently differentially expressed in 8 to 9 datasets (**Figure 7f**). Seven of these were receptors and one of these was *Neo1*, suggesting that Neo1 is one of the most consistently up-regulated genes found upon HSC ageing.

It has recently been established that surgical BM denervation mirrors the phenotype of arteriolar degeneration upon ageing and thereby induces premature HSC ageing[24]. Therefore, we tested whether the observed *Neo1* upregulation during HSC ageing (**Figure 7d**) or as a consequence of *Ntn1* deficiency (**Figure 6e**) was recapitulated upon denervation mediated induction of premature marrow ageing. One hind limb per Wt mouse was surgically denervated and LSK-SLAM cells 4 months after surgery were analysed. We found an increase in *Neo1* expression in HSCs of 7 out of 8 denervated femurs compared to sham-operated nerve-intact contralateral femurs of the same mice (**Figure 7g**). The *Neo1* up-regulation is consistent with a model that the normal or accelerated ageing process leads to a decrease in Ntn1 expression in the microenvironment, mediating a compensatory Neo1 up-regulation to maintain signalling when its ligand Ntn1 becomes limiting.

Finally, we investigated whether the niche mediated upregulation of *Neo1* in HSCs of 30 months old mice ($NTN1^{low}$ environment) can be reversed by transplanting them into two months old young mice ($NTN1^{high}$ environment). Indeed, *Neo1* expression in HSCs significantly decreased again in young mice (**Figure 7h**). These data further support the link between the level NTN1 production in the bone marrow microenvironment and expression of its receptor *Neo1* on HSCs in young and old mice (**Figure 7i**). However, the compensatory upregulation of *Neo1* expression due to age dependent ligand deprivation is not sufficient to maintain NEO1 function, since

366 ablation of either Ntn1 or Neo1 leads to proliferation and decreased self-renewal of
367 HSCs, a hallmark of aged HSCs.
368

Discussion

Here we identify arteriolar niche-derived NTN1 ligand and its cognate HSC specific receptor NEO1 as a novel ligand-receptor signalling axis regulating HSC quiescence and long-term self-renewal. This axis is deregulated upon aging and loss of either of its components leads to functional HSC impairment. NTN1-NEO1 represents a novel intercellular and non-cell autonomous signalling network by which NTN1 produced by perivascular niches binds to HSCs to fine-tune HSC dynamics, in particular cell cycle activity and long-term self-renewal.

In agreement with Neo1 being specifically expressed by dHSCs (**Figure 1**), *Neo1* is part of the *MoIO* signature marking functionally superior HSCs[50]. Expression of *Neo1* is also highest in Vwf^{+} HSCs residing on the top of the hematopoietic hierarchy[68] and NEO1+ cells have recently been reported as a subpopulation within Hoxb5+ HSCs[42]. Intriguingly, *Dnmt3a* mutant HSCs show increased quiescence, as well as a robust upregulation of *Neo1* expression[69-71] suggesting it as a potential target for *Dnmt3a* mutant hematopoietic disorders.

When characterizing *Neo1*-mutant hematopoiesis, we observed an initial increase in HSC numbers associated with loss of quiescence and subsequently loss of HSC self-renewal over time that correlated with decreased expression of *Egr1* and increased expression of *Cdk6*. Similarly, hematopoietic loss of *Egr1* leads to increased cycling and initial HSC expansion followed by a loss of engraftment potential upon serial transplantation[55]. Since we analysed a hypomorphic *Neo1* mouse model with severely decreased (>90%) but remaining minor expression[38, 47, 48], our results possibly underestimate the biological relevance of Neo1 in HSCs. It has been reported, that ≈ 80% of $Neo1^{gt/gt}$ mice die prenatally. The ones born develop hydrocephalus of varying degree, with around one in five displaying severe phenotypes with macroscopically visible “dome shaped” skulls [48]. Since this was reproducible in our analysis, we used only $Neo1^{gt/gt}$ mice without macroscopic features of hydrocephalus, which showed normal, healthy behavior. In these $Neo1^{gt/gt}$ mice, the HSC numbers were unchanged at the time of analysis. Nevertheless, we cannot formally exclude that additional factors such as neuronal stress may contribute to some extend to the described HSC phenotype in the primary $Neo1^{gt/gt}$ mutants.

NEO1 can bind multiple neural guidance molecules, which mediate context dependent effects. As an example, RGMs are known to inhibit neuronal migration[72],

while NTN1 acts as a chemoattractant for commissural axons[63]. In HSCs, we found NTN1, but neither RGMs nor BMP-2, to modulate HSC behaviour. This is intriguing, because in the developing bone, NEO1 modulates cartilage growth *via* canonical BMP signalling[73]. However, the relevance of BMP-signalling for adult HSCs remains uncertain[74].

Over the past years, the role of Netrins in neurobiology, originally established using gene trapped mice[62], has been challenged by novel conditional *Ntn1* alleles[63, 75, 76]. When we repurposed these to investigate hematopoiesis, we found increased activation and progressive loss of HSC numbers as well self-renewal potential after global deletion of *Ntn1,* mimicking the *Neo1* mutant phenotype. Further, *in vivo* overexpression and *in vitro* stimulation with NTN1 enhanced HSC quiescence and increased engraftment potential of cultured HSCs upon transplantation, respectively. These results, are in line with studies showing quiescence-inducing compounds that maintain HSC engraftment potential *in vitro*[11, 29, 77] as well as studies that associate loss of self-renewal capability *in vivo* with divisional history[13, 78, 79]. Altogether the data strongly suggest that NTN1 acts as a paracrine NEO1 ligand modulating HSC behaviour. Furthermore, Ntn1 has been described to support immature states of iPSCs and cancer stem cells[80, 81], suggesting it maintains stemness in various settings. Here, we demonstrate that NTN1/NEO1 signalling increase NF-κB activation in HSCs, a pathway known to protect HSCs from exhaustion during stress, while loss of p65 leads to hematopoietic failure[61, 82].

Within the bone marrow niche, we found *Ntn1* to be expressed in AECs and SMC in line with previous studies[65, 83, 84]. These, as well as other perivascular cells secrete multiple molecules that support HSCs including SCF and CXCL12[26, 27, 65, 83, 85, 86]. Upon aging, BM arterioles are remodelled leading to a depletion of periarteriolar stromal cells and SCF, affecting hematopoiesis[23-25]. In line, NTN1 secretion by SMCs is known to guide axons of the sympathetic nervous system (SNS) during arteriolar growth[66]. The connection between SNS and arterioles is intriguing, as denervation disrupts BM arterioles and mediates accelerated HSC ageing[24].

Our data strongly support the link between NTN1 production in the bone marrow microenvironment and expression of its receptor Neo1 on HSCs. Loss of *Ntn1* expression in the niches during: (a) physiological ageing, (b) accelerated aging by surgical denervation, or (c) by genetic ablation, results in compensatory upregulation

of *Neo1* expression due to ligand deprivation, which however is not sufficient to maintain Neo1 function. Such a mechanism has also been observed for the Ntn1 receptors DCC and NEO1 upon loss of *Ntn1* during development [76].

Collectively, our data suggest that NTN1 produced mainly by arteriolar niches preserves quiescence and self-renewal of HSCs via NEO1, while ageing associated decline of Ntn1 leads to the gradual decrease of Neo1 mediated HSC self-renewal.

ACKNOWLEDGEMENTS

We thank all technicians of the Trumpp, Mehlen and de Haan laboratories for technical assistance; S. Schmitt, M. Eich, K. Hexel, T. Rubner from the DKFZ Flow Cytometry Core, and W. Abdulahad, T. Bijma, G.Mesander and J. Teunis from UMCG Flowcytometry Unit facilities for their assistance; K. Reifenberg, P. Prückl, M. Schorpp-Kistner, A. Rathgeb and all members of the DKFZ and UMCG Laboratory Animal Core Facility for excellent animal welfare and husbandry. We thank the DKFZ and ERIBA Genomics and Proteomics Core Facility for their assistance. This work was supported by the Heinrich F.C. Behr foundation, Studienstiftung des deutschen Volkes (S.R), by INCA, ERC, ANR and Fondation Bettencourt (all to P.M.), Max Planck Society and the ERC-Stg-2017 (VitASTEM) (all to N.C-W), the FOR2033 and SFB873 funded by the Deutsche Forschungsgemeinschaft (DFG) and the Dietmar Hopp Foundation (all to A.T). Studies in the Frenette laboratory were funded by the National Institutes of Health (DK056638, HL069438, HL116340 to P.S.F.). M.M. is a New York Stem Cell Foundation (NYSCF) Druckenmiller fellow. Studies in the de Haan laboratory were funded by the Netherlands Organization for Scientific Research/Mouse Clinic for Cancer and Ageing, the Landsteiner Foundation for Blood Transfusion Research (LSBR1703), and Marriage, a EU FP7 Marie Curie Initial Training Network (Contract number 316964).

AUTHOR CONTRIBUTIONS

Conceptualization, S.R., N.C.-W. and A.T.; Methodology, S.R., A.F.S., J.P., N.R., P.S., L.L., S.L., M.M., B.G., A.R.R., D.Z., M.T., E.Z., B. D.-A., B.D., D.K., A.N., M.B., A.H.-W., K.S., C.K., P.Z., A.P., M.S.; Investigation, S.R., A.F.S., J.P., M.M., S.L., N.R.; Resources, M.H., P.M.; Writing – Original Draft, S.R., A.F.S., N.C.-W. and A.T.; Writing – Review and Editing, S.R., A.F.S., J.P., P.S., L.L., N.R., M.M., S.M., P.S.F., M.H., L.B., P.M., G.d.H., N.C.-W. and A.T.; Supervision, G.d.H. N.C.-W. and A.T.

DECLARATION OF INTERESTS

The authors declare no competing interests.

METHODS

CONTACT FOR REAGENT AND RESOURCE SHARING

Further information and requests for resources and reagents should be directed to and will be fulfilled by the Lead Contact, Andreas Trumpp a.trumpp@dkfz.de. Certain materials are shared with research organizations for research and educational purposes only under an MTA to be discussed in good faith with the recipient.

EXPERIMENTAL MOUSE MODELS

SCL-tTA; H2B-GFP mice: This transgenic mouse line, expresses the fusion protein histone H2B-GFP under the tetracycline-responsive regulatory element and the tTA-S2 transactivator from the endogenous *Scl* locus (Wilson et al., 2008). Doxycycline was supplemented in drinking water of 8 - 16 weeks old mice for 150 as previously described (Wilson et al., 2008). To set the gates for GFP+ cells, age-matched *H2B-GFP* littermates were used. *SCL-tTA; H2B-GFP* mice were backcrossed to C57BL/6J.

C57BL/6J (CD45.2, CD45.1 or CD45.2/CD45.1) mice were either purchased from Envigo (the Netherlands) or Janvier Labs (France) or bred in-house.

Gprc5c-GFP mice (*Tg(Gprc5c-EGFP)JU90Gsat*): This transgenic mouse line was previously generated by inserting an EGFP gene into a BAC clone at the initiating ATG codon of the first coding exon of the *Gprc5c* gene and this BAC clone was subsequently used to generate transgenic reporter mice (Gong et al., 2003). Analyzed mice were backcrossed to C57BL/6J.

Myc-eGFP mice: This transgenic mouse line expresses a fusion protein of c-Myc and eGFP (Huang et al., 2008).

FUCCI mice *(B6-Tg(Gt(ROSA)26Sor-Fucci2)#Sia*): This transgenic mouse line allows identification of cell cycle phase via fluorescent fusion proteins, mice were sacrificed after 8 - 16 weeks (Sakaue-Sawano; et al., 2008).

Neo1$^{gt/gt}$ mice (*B6.129P2-Neo1*$^{Gt(KST265)Byg/Mmmh}$): These mice harbour a gene-trapped *Neo1* allele that leads to a strong reduction of *Neo1* expression (Leighton et al., 2001). For transplantation experiments, male and female animals 4 - 6 weeks of age were used. Control transplantations were always performed using gender matched, wild-type littermates. For competitive transplantations, competitor bone marrow (BM) was also age and gender matched.

Ntn1$^{ßgeo/+}$ mice (*Ntn1*$^{Gt(ST629)Byg}$): These mice harbour a gene-trapped *Ntn1* allele that leads to a strong reduction of *Ntn1*. Heterozygous mice can be used as reporter mice employing the ß-gal reporter in the gene-trap vector (Serafini et al.; 1996).

Ntn1$^{fl/fl}$ mice: This transgenic mouse line contains loxP sites flanking coding sequences containing both the principal ATG (based on *Ntn1* cDNA sequence NM_008744) and the cryptic ATG (based on *Ntn1* cDNA: BC141294) and the alternative promoter described in intron 3 (Dominici et al., 2017). To generate global *Ntn1* deletion we crossed *Ntn1*$^{fl/fl}$ mice to *CAGGS-Cre*^{ERT2} mice (Jackson laboratories). For smooth muscle specific deletion, *Ntn1*$^{fl/fl}$ mice were crossed to *Sma-Cre*^{ERT2} mice. For 8 weeks endpoints *Ntn*$^{fl/fl}$ crossings only female and for 5 months endpoints, only male mice were analyzed to reduce variability.

+ / LSL-Rosa26-Ntn1 mice: This transgenic mouse line was generated for this study. The human *NETRIN-1* was cloned in Rosa26-lox-stop-lox plasmid (Soriano). Mice were

generated by SEAT CNRS Gustave Roussy phenomin. We crossed these mice to *CAGGS:Cre^{ERT2}* mice (Jackson laboratories), inducing global overexpression of Ntn1. To reduce variability, only male animals were analyzed at 5 month after Cre induction.

Sma-RFP mice (*C.Cg-Tg(aSMA-RFP)#Rkl*): The mouse line harbours a RFP reporter for *smooth muscle actin* (*Sma*) and thereby allows identification of smooth muscle cells (LeBleu et al., 2013). *Sma-RFP* mice are on a BALB/C background.

All other mouse models are on a B6J background.

All mice were bred in-house in the animal facilities of DKFZ, University Medical Center Groningen, INSERM or Albert-Einstein College of medicine under specific pathogen free (SPF) conditions in individually ventilated cages (IVC) at 24 degrees, a humiditiy of 80% with fixed day/night cycles of 12 hours. According to German, French, American or Dutch guidelines, mice were euthanized by cervical dislocation and all animal procedures were performed according to protocols approved by the Regierungspräsidium Karlsruhe, Animal Care and Use Committee of Albert Einstein College of Medicine, the Instantie voor Dierenwelzijn (IvD) committee, Universitair Medisch Centrum Groningen/Rijksuniversiteit Groningen or University of Lyon local Animal Ethic Evaluation Committee. To reduce animal numbers, remaining BM / cDNA samples generated in this and previous studies were used whenever possible.

METHOD DETAILS

pIC- or LPS-Induced Inflammatory Stress

Mice were injected intraperitoneally with pIC (100 µg/Mouse in 0.1 ml PBS), LPS (5 µg / mouse in 0.1 ml PBS) or PBS alone. 16 hours (LPS / pIC / PBS), 5 or 8 days (pIC / PBS) later, mice were sacrificed and BM cells were used for subsequent analysis.

Cell Isolation and Flow Cytometry

Mouse BM cells were isolated, and HSCs and MPP1-4 progenitors defined by immune-phenotype (Lineage$^-$, Sca1$^+$, c-Kit$^+$, CD135$^{-/+}$, CD150$^{-/+}$, CD48$^{-/+}$, CD34$^{-/+}$, CD45.2 CD45.1/2, CD45.1) (see also **Figure 1A**), or LSK-SLAM (Lineage$^-$ c-Kit$^+$ CD150$^+$ CD48$^-$) purified by FACS and subsequently subjected to RNA-seq, population qPCR analysis, *in vitro* experiments, reconstitution assays or cytological analysis. Briefly, BM was isolated from pooled femora, tibiae, ilia and vertebrae by gentle crushing in PBS using a mortar and pistil. If no depletion of lineage-positive cells was performed, lysis of erythrocytes was performed using ACK Lysing Buffer (Thermo Fisher Scientific). To deplete lineage-positive cells we used the Dynabeads Untouched Mouse CD4 Cells Kit (Invitrogen). Briefly, total BM was stained for 30 min with 100µl / mouse of the Lineage Cocktail provided in the Dynabeads

Untouched Mouse CD4 Cells Kit (Invitrogen) in PBS. Labelled cells were then incubated for 20 min with 1.5 ml / mouse of washed polyclonal sheep anti-rat IgG coated Dynabeads provided in the Kit. Cells were depleted using a magnet, enriching for the lineage-negative (Lineage$^-$) cell fraction. To purify HSC and MPP1-4, the Lineage$^-$ fraction was stained for 30 min using the following monoclonal antibodies: anti-lineage [anti-CD4 (clone GK1.5), anti-CD8a (53-6.7), anti-CD11b (M1/70), anti- B220 (RA3-6B2), anti-GR1 (RB6-8C5) and anti-TER119 (Ter-119)]; anti-CD117/c-Kit (2B8); anti-Ly6a/Sca-1 (D7); anti-CD34 (RAM34); anti-CD150 (TC15-12F12.2); anti-CD48 (HM48-1); anti-CD135 (A2F10); CD45.1 (A20); CD45.2 (104). The coupled fluorochromes used depended on the experiment to allow sorting of different fluorescent protein containing reporters or isolation of HSC from transplants. Monoclonal antibody conjugates were purchased from eBioscience, BD Bioscience or BioLegend. Cell sorting was then performed on a FACS Aria I, II and III, FACS Aria Fusion (Becton Dickinson) using BD FACSDiva v8.0.3 (BD Bioscience) or MoFlo Astrios or XDP cell sorters (Beckman Coulter). Sorted in Complete Stem Cell Medium (specified elsewhere) for *in vitro* culture, cytology and reconstitution experiments, or RNA lysis buffer (ARCTURUS PicoPure RNA Isolation Kit (Life Technologies, Invitrogen) for population RNA-seq or qPCR and stored at -80 °C.

For Figure S4c LT-HSCs were characterized as Lin$^-$Sca-1$^+$c-Kit$^+$CD48$^-$CD150$^+$, ST-HSCs as Lin$^-$Sca-1$^+$c-Kit$^+$CD48$^-$CD150$^-$ and MPPs as Lin$^-$Sca-1$^+$c-Kit$^+$CD48$^+$CD150$^-$. For isolation of committed progenitor subsets the following markers were used for isolation: CLP (Lin$^-$CD127$^+$Sca-1^{lo}c-Kit^{lo}), CMP (Lin$^-$CD127$^-$Sca$^-$1$^-$c-Kit$^-$CD34$^+$CD16/CD32^{hi}), GMP (Lin$^-$CD127$^-$Sca$^-$1-c-Kit$^+$CD16/CD32^{hi}), and MEP (Lin$^-$CD127$^-$Sca-1$^-$c-Kit$^+$CD34$^-$CD16/CD32$^+$). Data was analysed using FlowJo, Versions 6-10.5.3.

CDK6/ NEO1 Staining

For analyses of NEO1 expression BM cells were isolated from mice and stained for HSC/MPP markers an sorted as described. Cells were plated on poly-L-Lysine coated slides and then fixed with BD Cytofix/Cytoperm Buffer (Beckton Dickinson). Subsequently, Cdk6 (Abcam) or Neo1 (Abcam) staining was performed in 0.1% Triton (Sigma) and 5% BSA. Secondary antibodies coupled to AF-488 were used. After washing, slides were embedded in anti fade reagent with DAPI (Invitrogen) and imaging was performed employing a Zeiss LSM 700 or LSM 710 confocal microscope using ZEN blue v2.5 (Zeiss international). Experimental replicates were always performed side by side and imaged in one session without change of laser intensities or gain to avoid technical bias and allow comparability. DAPI signal was not used for quantification or normalisation. Analysis was performed with FIJI v.2.0.

NEO1 Staining - Figure 7e

4000-6000 LT-HSCs were seeded in spots of an immunofluorescent adhesion slide (VWR) and allowed to settle for 20 minutes. Cells were then fixed and permeabilized with Fixation and Permeabilization Solution (BD Biosciences) for 20 minutes on ice. Cells were then blocked with 4% BSA for 30 minutes at room temperature and then stained with 1:100 Mouse Neo1 biotinylated antibody (R&D) at 4°C. Cells were washed three times in 0.1% Tritox-X-100 PBS solution and stained with 1:500 secondary antibody streptavidin Alexa-647 for one hour at 4 °C. After washing, coverslips were mounted in anti-fade reagent with DAPI (Invitrogen).

p65-GFP-Staining

After 48 hours of culture of 2000 HSCs/well, cells were plated on poly-L-Lysine coated slides and then fixed with BD Cytofix/Cytoperm Buffer (Beckton Dickinson). Subsequently, anti-GFP-488 (Abcam) staining was performed in 0.1% Triton (Sigma) 5% BSA for 1 hours to increase signal. After washing, coverslips were mounted in anti-fade reagent with DAPI (Invitrogen).

Cell Cycle Analysis

HSC/MPP surface staining (LSK, CD150, CD48, CD34) was performed on BM cells or *in vitro* treated HSPCs. Cells were fixed with BD Cytofix/Cytoperm Buffer (Beckton Dickinson). Subsequently, intracellular Ki-67 (BD Biosciences) staining was performed using PermWash solution (Beckton Dickinson). Prior to flow cytometry analysis cells were stained with Hoechst 33342 (Invitrogen) or DAPI (ThermoFisher).

Population RNA-seq

For Figures 4e-j and S2c-e: Population RNA-seq data was generated as previously described (Cabezas-Wallscheid et al., 2014). Briefly, total RNA isolation was performed using ARCTURUS PicoPure RNA Isolation Kit (Life Technologies, Invitrogen) according to the manufacturer's instructions. Total RNA was used for quality controls and for normalization of starting material. cDNA-libraries were generated using 1 ng of total RNA for *Neo1* deficient / wtildtype HSCs using the SMARTer Ultra Low RNA Kit for Illumina Sequencing (ClonTech) according to the manufacturer's indications. Sequencing was performed using the HiSeq2000 device (Illumina).

RNA-seq – Young and Old LSK-SLAM for figures 7d, S4d

RNA was isolated from 15000 LSK-SLAM cells ($Lin^-Sca1^+c\text{-}Kit^+CD48^-CD150^+$) using the Nucleospin XS kit (Macherey Nagel) and quantified on Bionalyzer using RNA Pico 6000 Kit (Agilent). Ribosomal depletion was performed using a modified version of RiboZero Kit (Illumina). 300 pg ribosomal-depleted RNA was used as input into TotalScript RNA-Seq Kit (Epicentre). Libraries were pooled and sequenced to 30-50 million reads on HiSeq 2500.

qPCR-Analysis

For quantitative Real-time PCR, total RNA of 2000-10000 cells was isolated as described above or using Nucleospin RNA XS Kit (Machery Nagel) and reverse-transcribed using SuperScript VILO cDNA Synthesis Kit (Invitrogen) according to manufacturer's guidelines. For qPCR analysis, Fast SYBR Green Master Mix (Thermo Scientific) or LightCycler SYBR Green I (Roche) was used on a ViiA 7 Real- Time PCR System (Applied Biosystems) or a LightCycler 480 Instrument (Roche). RNA expression was normalized to *Oaz1, Act2b* or *Hprt* housekeeping gene expression and presented as relative quantification (Ratio = 2^-DDCT). Primers were designed using the Universal ProbeLibrary Assay Design Center (Roche) or ncbi Primer-BLAST (ncbi) and ordered from Sigma. Primer sequences are available in the Supplemental Information file.

Reconstitution Experiments

For generation of full chimeras, 3x10^6 total BM cells from 4 week old wildtype CD45.2 or *Neo1*$^{gt/gt}$ CD45.2 mice were injected per recipient mouse.

For generation of 50/50 Chimeras 1.5x10^6 total BM cells from 4 week old wildtype CD45.2 or *Neo1*$^{gt/gt}$ CD45.2 mice were mixed with 1.5x10^6 total BM cells derived from CD45.1/2 mice so that a total of 3x10^6 BM cells was injected per recipient mouse.

For transplantation after *in vitro* treatment, 500 sorted HSCs of CD45.1/2 or CD45.2 derived from 8 - 12 weeks old animals were cultured for 48 h in respective conditions. Then a well of progeny of CD45.1/.2 was mixed to a well of progeny of CD45.2 and then transplanted. A similar setup was used for the assessment of *Neo1* dependency of *in vitro Netrin-1* treatment: 500 *Neo1*-deficient $CD45.2^+$ HSCs were sorted after 8 month from old *Neo1* full chimeras and then incubated with or without Ntn1. These *Neo1*-deficient HSCs were mixed with 500 CD45.1/2 HSC incubated without Netrin-1, derived from 8 weeks old CD45.1/2 animals and then transplanted into individual recipients.

For secondary transplantations, 3x10^6 total BM cells were isolated and transplanted.

For potency assessment of 100/500 CD45.2 wildtype or *Neo1*-mutant HSCs were sorted from straight chimeras 15 months after transplantation, mixed with 1x10^5 total BM cells from 8-12 weeks old CD45.1/.2 mice and transplanted.

For assessment of HSC homing 10 x10^3 LSK cells derived from CD45.2 wildtype or *Neo1* deficient mice were sorted and transplanted.

For generation of 50/50 Chimeras 1.5x10^6 total BM cells from 6,5 month old Ntn1-OE/ $Ntn1^{\Delta CAGGSCre/\Delta CAGGSCre}$ or CAGGS-Cre mice, were mixed with 1.5x10^6 total BM cells derived from CD45.1/2 mice so that a total of 3x10^6 BM cells was injected per recipient mouse.

For transplantations of sorted HSC, 200 HSC from 6,5 month old $Ntn1^{\Delta CAGGSCre/\Delta CAGGSCre}$ or CAGGS-Cre were mixed with 1x10^6 total spleen cells from CD45.1/2 mice and injected into the recipient.

For transplantation of 30 month old HSC, 3x10^6 total bone marrow cells were isolated and injected into recipients.

For all experiments, cells were transplanted into fully irradiated (2 x 5 Gy) B6J mice (CD45.1). Contribution of CD45.2 or CD45.1/.2-donor cells was monitored in peripheral blood approximately every 4 weeks post-transplantation in all transplantations using either LSRII, LSR Fortessa.

Outcome was addressed by absolute blood counts or flow cytometry using the following monoclonal antibodies: anti-CD45.1 (A20); anti-CD45.2 (104); anti-CD4 (clone GK1.5), anti-CD8a (53-6.7), anti-CD11b (M1/70), anti-B220 (RA3-6B2), anti-GR1 (RB6-8C5). The applied fluorochromes depended on the experiment. For endpoint analysis of chimera animals, BM stainings were performed as following: anti-lineage [anti-CD4 (clone GK1.5), anti-CD8a (53-6.7), anti-CD11b (M1/70), anti- B220 (RA3-6B2), anti-GR1 (RB6-8C5) and anti-TER119 (Ter-119)]; anti-CD117/c-Kit (2B8); anti-Ly6a/Sca-1 (D7; anti-CD34 (RAM34); anti-CD150 (TC15-12F12.2-; anti-CD48 (HM48-1); anti-CD45.1 (A20); anti-CD45.2 (104). Monoclonal antibody conjugates were purchased from eBioscience, BD bioscience or BioLegend.

Tamoxifen induction schema

For *Sma*:Cre^{ERT2}; $Ntn1^{fl/fl}$, *CAGGS:*Cre^{ERT2}; $Ntn1^{fl/fl}$ $Ntn1^{fl/fl}$ and *CAGGS:*Cre^{ERT2}*;LSL-Rosa26-Ntn1 mice* 3 Tamoxifen (Sigma-Aldrich) injections in 1 week were performed 4 - 6 weeks old animals. 8 weeks or 5 months after Cre induction mice were sacrificed and analyzed.

BrdU analysis

Full chimeras of *Neo1*-mutant or wildtype CD45.2 BM were injected intraperitoneally with 0.2 ml BrdU (1.8 mg/ml; Sigma) 4 months after transplantation and sacrificed 48 h after injection. Then HSC surface staining was performed as described above, cells were processed and then staining with anti-BrdU (BD Bioscience) antibody (1:30) was performed.

HSPCs plating and in vitro treatment

5000 LSK-SLAM cells for RNA analysis, or 5000-10000 HSCs for imaging or cell cycle analysis were sorted into and then cultured in Complete Stem Cell Medium (StemPro-34 SFM, LifeTechnologies containing 50 ng/ml SCF and 25 ng/ml TPO (all Preprotech), 100 u/ml Penicillin/Streptomycin, 2 mM L-Glutamine, StemPro-34 Supplement as recommended). Cells were cultured in 96-well ultralow attachment plates (Corning) and were treated with either recombinant 1 µl/ml Ntn-1 (R&D), 1 µl/ml Rgm-a (R&D), 1 µl/ml Rgm-b (R&D) or 200 ng/ml Bmp-2 (R&D) in addition to the standard cytokines. Concentration of JSH-23 was 6µM. 48 hours after plating, cells were used for downstream procedures such as RNA isolation, imaging or flow cytometry as described in its respective chapter.

Bone marrow denervation by transaction of femoral and sciatic nerves

Denervation of the femoral and tibial BM was done as previously described (Maryanovich et al., 2018). The femoral nerve was localized after its exit from the vertebral column deep in the psoas muscle. This was accomplished with a midline abdominal incision; the intestines were gently moved aside to visualize the psoas muscle. An incision was made in the psoas to visualize the femoral nerve, and a 1 cm section of the nerve was excised. Deep to the psoas (through the incision), the sciatic nerve was visualized in close proximity to the iliac crest of the pelvis, and a 1 cm section of the nerve was excised. For sham operation, both femoral and sciatic nerves were exposed by surgery, but were left intact.

Bone marrow digestion for stromal cell isolation

For isolation of stromal cells, we thoroughly cleaned dissected bones, crushed and digested them for 1 h in RPMI with 2% FCS as well as 0.25% Collagenase Type I (Gibco). After digestion was stopped with 10% FCS containing medium, red cell lyses, lineage depletion, staining and cell sorting were performed as described above.

QUANTIFICATION, STATISTICS AND REPRODUCIBILITY

Standard quantifications, display and experimental design

Statistical analysis was performed with two-tailed paired Student's t-test or Two-way-ANOVA using Fishers LSD for multiple comparisons as indicated in the respective figure legend. All data are presented as mean +SD. For box and whiskers plots, error bars depict min to max values, the box is defined at 25^{th}-75^{th} percentile and the median is marked with an additional line. Please see Figure Legends for detailed information. GraphPad Prism 7/8 was used for statistical analysis. The number of independent experiments is indicated in the respective Figure Legends. Sample exclusion was only done as a result of premature mouse death, infection, or clear mistakes in sample processing.

RNA-Sequencing analysis

For RNA-seq of *Neo1-mutant* and control HSCs, the following pipeline was used: Sequenced read fragments were mapped to the mouse reference genome GRCm38 using STAR (STAR_2.6.1a) (Dobin et al., 2013). Expression counts estimates were generated using HTSeq (htseq-0.9.1) (Anders et al., 2015). DESeq2 (DESeq2_1.20.0) (Love et al., 2014) was used to test for differential expression; results were considered significant at a p.adj. value < 0.05. Analysis was performed in R-studio v3.5.2 (www.r-project.org).

For Figure 7d,f and S4d, differential expression was calculated using egdeR (3.24.3).

Downstream analysis

Gene set enrichment analysis was performed using GSEA software (3.0) on pre-ranked differential expression lists.

REPORTING SUMMARY

Further information on experimental design is available in the Nature Research Reporting Summary.

DATA AVAILABILITY STATEMENT

RNA-seq data has been deposited in online repositories: Data linked to Figure 4: MTAB-7902, data linked to Figure 7: GSE128050. Expression data from young and old *Neo1*-mutant or control HSC can be found in Supplemental Data file 1. Expression data from the analysis of young and old LSK-SLAM cells can be found in Supplemental Data file 2.

Source data for all 7 Figures and 4 Supplementary Figures is available in Supplemental Data file 3. Nucleotide sequences and additional source data is available upon reasonable request to the corresponding author.

References

1. Cabezas-Wallscheid, N. *et al.* Identification of regulatory networks in HSCs and their immediate progeny via integrated proteome, transcriptome, and DNA methylome analysis. *Cell Stem Cell* **15**, 507-522 (2014).
2. Kiel, M.J. *et al.* SLAM Family Receptors Distinguish Hematopoietic Stem and Progenitor Cells and Reveal Endothelial Niches for Stem Cells. *Cell* **121**, 1109-1121 (2005).
3. Pietras, E.M. *et al.* Functionally Distinct Subsets of Lineage-Biased Multipotent Progenitors Control Blood Production in Normal and Regenerative Conditions. *Cell Stem Cell* **17**, 35-46 (2015).
4. Busch, K. *et al.* Fundamental properties of unperturbed haematopoiesis from stem cells in vivo. *Nature* **518**, 542-546 (2015).
5. Rodriguez-Fraticelli, A.E. *et al.* Clonal analysis of lineage fate in native haematopoiesis. *Nature* **553**, 212-216 (2018).
6. Benz, C. *et al.* Hematopoietic stem cell subtypes expand differentially during development and display distinct lymphopoietic programs. *Cell Stem Cell* **10**, 273-283 (2012).
7. Purton, L.E. & Scadden, D.T. Limiting factors in murine hematopoietic stem cell assays. *Cell Stem Cell* **1**, 263-270 (2007).
8. Till, J.E. & McCulloch, E.A. A direct measurement of the radiation sensitivity of normal mouse bone marrow cells. *Radiat Res* **14**, 213-222 (1961).
9. Yamamoto, R. *et al.* Clonal analysis unveils self-renewing lineage-restricted progenitors generated directly from hematopoietic stem cells. *Cell* **154**, 1112-1126 (2013).
10. Wilson, A. *et al.* Hematopoietic stem cells reversibly switch from dormancy to self-renewal during homeostasis and repair. *Cell* **135**, 1118-1129 (2008).
11. Cabezas-Wallscheid, N. *et al.* Vitamin A-Retinoic Acid Signaling Regulates Hematopoietic Stem Cell Dormancy. *Cell* **169**, 807-823.e819 (2017).
12. Foudi, A. *et al.* Analysis of histone 2B-GFP retention reveals slowly cycling hematopoietic stem cells. *Nat Biotechnol* **27**, 84-90 (2009).
13. Bernitz, J.M., Kim, H.S., MacArthur, B., Sieburg, H. & Moore, K. Hematopoietic Stem Cells Count and Remember Self-Renewal Divisions. *Cell* **167**, 1296-1309 e1210 (2016).
14. Sudo, K., Ema, H., Morita, Y. & Nakauchi, H. Age-Associated Characteristics of Murine Hematopoietic Stem Cells. *The Journal of Experimental Medicine* **192**, 1273-1280 (2000).
15. Dykstra, B., Olthof, S., Schreuder, J., Ritsema, M. & de Haan, G. Clonal analysis reveals multiple functional defects of aged murine hematopoietic stem cells. *J Exp Med* **208**, 2691-2703 (2011).
16. Verovskaya, E. *et al.* Heterogeneity of young and aged murine hematopoietic stem cells revealed by quantitative clonal analysis using cellular barcoding. *Blood* **122**, 523-532 (2013).
17. Sawen, P. *et al.* Murine HSCs contribute actively to native hematopoiesis but with reduced differentiation capacity upon aging. *Elife* **7** (2018).
18. Yamamoto, R. *et al.* Large-Scale Clonal Analysis Resolves Aging of the Mouse Hematopoietic Stem Cell Compartment. *Cell Stem Cell* **22**, 600-607 e604 (2018).
19. Geiger, H., de Haan, G. & Florian, M.C. The ageing haematopoietic stem cell compartment. *Nature Reviews Immunology* **13**, 376-389 (2013).

20. Sun, D. *et al.* Epigenomic profiling of young and aged HSCs reveals concerted changes during aging that reinforce self-renewal. *Cell Stem Cell* **14**, 673-688 (2014).
21. Beerman, I. *et al.* Proliferation-dependent alterations of the DNA methylation landscape underlie hematopoietic stem cell aging. *Cell Stem Cell* **12**, 413-425 (2013).
22. Florian, M.C. *et al.* Cdc42 activity regulates hematopoietic stem cell aging and rejuvenation. *Cell Stem Cell* **10**, 520-530 (2012).
23. Kusumbe, A.P. *et al.* Age-dependent modulation of vascular niches for haematopoietic stem cells. *Nature* **532**, 380-384 (2016).
24. Maryanovich, M. *et al.* Adrenergic nerve degeneration in bone marrow drives aging of the hematopoietic stem cell niche. *Nat Med* **24**, 782-791 (2018).
25. Ho, Y.H. *et al.* Remodeling of Bone Marrow Hematopoietic Stem Cell Niches Promotes Myeloid Cell Expansion during Premature or Physiological Aging. *Cell Stem Cell* (2019).
26. Morrison, S.J. & Scadden, D.T. The bone marrow niche for haematopoietic stem cells. *Nature* **505**, 327-334 (2014).
27. Pinho, S. & Frenette, P.S. Haematopoietic stem cell activity and interactions with the niche. *Nat Rev Mol Cell Biol* **20**, 303-320 (2019).
28. Chen, X. *et al.* Bone Marrow Myeloid Cells Regulate Myeloid-Biased Hematopoietic Stem Cells via a Histamine-Dependent Feedback Loop. *Cell Stem Cell* **21**, 747-760 e747 (2017).
29. Hur, J. *et al.* CD82/KAI1 Maintains the Dormancy of Long-Term Hematopoietic Stem Cells through Interaction with DARC-Expressing Macrophages. *Cell Stem Cell* **18**, 508-521 (2016).
30. Duchene, J. *et al.* Atypical chemokine receptor 1 on nucleated erythroid cells regulates hematopoiesis. *Nat Immunol* **18**, 753-761 (2017).
31. Yoshihara, H. *et al.* Thrombopoietin/MPL signaling regulates hematopoietic stem cell quiescence and interaction with the osteoblastic niche. *Cell Stem Cell* **1**, 685-697 (2007).
32. Zou, Y.R., Kottmann, A.H., Kuroda, M., Taniuchi, I. & Littman, D.R. Function of the chemokine receptor CXCR4 in haematopoiesis and in cerebellar development. *Nature* **393**, 595-599 (1998).
33. Molineux, G., Migdalska, A., Szmitkowski, M., Zsebo, K. & Dexter, T.M. The Effects on Hematopoiesis of Recombinant Stem-Cell Factor (Ligand for C-Kit) Administered Invivo to Mice Either Alone or in Combination with Granulocyte Colony-Stimulating Factor. *Blood* **78**, 961-966 (1991).
34. Siebold, C., Yamashita, T., Monnier, P.P., Mueller, B.K. & Pasterkamp, R.J. RGMs: Structural Insights, Molecular Regulation, and Downstream Signaling. *Trends Cell Biol* **27**, 365-378 (2017).
35. Mirakaj, V., Jennewein, C., Konig, K., Granja, T. & Rosenberger, P. The guidance receptor neogenin promotes pulmonary inflammation during lung injury. *FASEB J* **26**, 1549-1558 (2012).
36. Schlegel, M. *et al.* Inhibition of neogenin fosters resolution of inflammation and tissue regeneration. *J Clin Invest* **128**, 4711-4726 (2018).
37. Muramatsu, R. *et al.* RGMa modulates T cell responses and is involved in autoimmune encephalomyelitis. *Nat Med* **17**, 488-494 (2011).
38. Leighton, P.A. *et al.* Defining brain wiring patterns and mechanisms through gene trapping in mice. *Nature* **410**, 174-179 (2001).

39. Xu, K. *et al.* Neural migration. Structures of netrin-1 bound to two receptors provide insight into its axon guidance mechanism. *Science* **344**, 1275-1279 (2014).
40. Healey, E.G. *et al.* Repulsive guidance molecule is a structural bridge between neogenin and bone morphogenetic protein. *Nat Struct Mol Biol* **22**, 458-465 (2015).
41. Lee, N.K. *et al.* Neogenin recruitment of the WAVE regulatory complex maintains adherens junction stability and tension. *Nat Commun* **7**, 11082 (2016).
42. Gulati, G.S. *et al.* Neogenin-1 distinguishes between myeloid-biased and balanced Hoxb5 (+) mouse long-term hematopoietic stem cells. *Proc Natl Acad Sci U S A* **116**, 25115-25125 (2019).
43. Forsberg, E.C. *et al.* Differential expression of novel potential regulators in hematopoietic stem cells. *PLoS Genet* **1**, e28 (2005).
44. Nestorowa, S. *et al.* A single-cell resolution map of mouse hematopoietic stem and progenitor cell differentiation. *Blood* **128**, e20-31 (2016).
45. Essers, M.A. *et al.* IFNalpha activates dormant haematopoietic stem cells in vivo. *Nature* **458**, 904-908 (2009).
46. Baldridge, M.T., King, K.Y., Boles, N.C., Weksberg, D.C. & Goodell, M.A. Quiescent haematopoietic stem cells are activated by IFN-gamma in response to chronic infection. *Nature* **465**, 793-797 (2010).
47. Bae, G.U. *et al.* Neogenin Regulates Skeletal Myofiber Size and Focal Adhesion Kinase and Extracellular Signal-regulated Kinase Activities In Vivo and In Vitro. *Mol Biol Cell* **20**, 4920-4931 (2009).
48. O'Leary, C.J. *et al.* Neogenin Recruitment of the WAVE Regulatory Complex to Ependymal and Radial Progenitor Adherens Junctions Prevents Hydrocephalus. *Cell Rep* **20**, 370-383 (2017).
49. Venezia, T.A. *et al.* Molecular signatures of proliferation and quiescence in hematopoietic stem cells. *PLoS Biol* **2**, e301 (2004).
50. Wilson, Nicola K. *et al.* Combined Single-Cell Functional and Gene Expression Analysis Resolves Heterogeneity within Stem Cell Populations. *Cell Stem Cell* **16**, 712-724 (2015).
51. Haas, S. *et al.* Inflammation-Induced Emergency Megakaryopoiesis Driven by Hematopoietic Stem Cell-like Megakaryocyte Progenitors. *Cell Stem Cell* **17**, 422-434 (2015).
52. Zhao, M. *et al.* N-Cadherin-Expressing Bone and Marrow Stromal Progenitor Cells Maintain Reserve Hematopoietic Stem Cells. *Cell Rep* **26**, 652-669 e656 (2019).
53. Laurenti, E. *et al.* CDK6 levels regulate quiescence exit in human hematopoietic stem cells. *Cell Stem Cell* **16**, 302-313 (2015).
54. Scheicher, R. *et al.* CDK6 as a key regulator of hematopoietic and leukemic stem cell activation. *Blood* **125**, 90-101 (2015).
55. Min, I.M. *et al.* The transcription factor EGR1 controls both the proliferation and localization of hematopoietic stem cells. *Cell Stem Cell* **2**, 380-391 (2008).
56. Galloway, A. *et al.* RNA-binding proteins ZFP36L1 and ZFP36L2 promote cell quiescence. *Science* **352**, 453-459 (2016).
57. Deneault, E. *et al.* A functional screen to identify novel effectors of hematopoietic stem cell activity. *Cell* **137**, 369-379 (2009).
58. Adelman, E.R. *et al.* Aging Human Hematopoietic Stem Cells Manifest Profound Epigenetic Reprogramming of Enhancers That May Predispose to Leukemia. *Cancer Discov* **9**, 1080-1101 (2019).

59. Sakaue-Sawano, A. *et al.* Visualizing spatiotemporal dynamics of multicellular cell-cycle progression. *Cell* **132**, 487-498 (2008).
60. Huang, C.Y., Bredemeyer, A.L., Walker, L.M., Bassing, C.H. & Sleckman, B.P. Dynamic regulation of c-Myc proto-oncogene expression during lymphocyte development revealed by a GFP-c-Myc knock-in mouse. *Eur J Immunol* **38**, 342-349 (2008).
61. Yamashita, M. & Passegue, E. TNF-alpha Coordinates Hematopoietic Stem Cell Survival and Myeloid Regeneration. *Cell Stem Cell* **25**, 357-372 e357 (2019).
62. Serafini, T. *et al.* Netrin-1 is required for commissural axon guidance in the developing vertebrate nervous system. *Cell* **87**, 1001-1014 (1996).
63. Dominici, C. *et al.* Floor-plate-derived netrin-1 is dispensable for commissural axon guidance. *Nature* **545**, 350-354 (2017).
64. Guo, C., Yang, W. & Lobe, C.G. A Cre recombinase transgene with mosaic, widespread tamoxifen-inducible action. *Genesis* **32**, 8-18 (2002).
65. Xu, C. *et al.* Stem cell factor is selectively secreted by arterial endothelial cells in bone marrow. *Nat Commun* **9**, 2449 (2018).
66. Brunet, I. *et al.* Netrin-1 controls sympathetic arterial innervation. *J Clin Invest* **124**, 3230-3240 (2014).
67. LeBleu, V.S. *et al.* Identification of human epididymis protein-4 as a fibroblast-derived mediator of fibrosis. *Nat Med* **19**, 227-231 (2013).
68. Sanjuan-Pla, A. *et al.* Platelet-biased stem cells reside at the apex of the haematopoietic stem-cell hierarchy. *Nature* **502**, 232-236 (2013).
69. Challen, G.A. *et al.* Dnmt3a is essential for hematopoietic stem cell differentiation. *Nat Genet* **44**, 23-31 (2011).
70. Challen, G.A. *et al.* Dnmt3a and Dnmt3b have overlapping and distinct functions in hematopoietic stem cells. *Cell Stem Cell* **15**, 350-364 (2014).
71. Jeong, M. *et al.* Loss of Dnmt3a Immortalizes Hematopoietic Stem Cells In Vivo. *Cell Rep* **23**, 1-10 (2018).
72. Monnier, P.P. *et al.* RGM is a repulsive guidance molecule for retinal axons. *Nature* **419**, 392-395 (2002).
73. Zhou, Z. *et al.* Neogenin regulation of BMP-induced canonical Smad signaling and endochondral bone formation. *Dev Cell* **19**, 90-102 (2010).
74. Singbrant, S. *et al.* Canonical BMP signaling is dispensable for hematopoietic stem cell function in both adult and fetal liver hematopoiesis, but essential to preserve colon architecture. *Blood* **115**, 4689-4698 (2010).
75. Yung, A.R., Nishitani, A.M. & Goodrich, L.V. Phenotypic analysis of mice completely lacking netrin 1. *Development* **142**, 3686-3691 (2015).
76. Bin, J.M. *et al.* Complete Loss of Netrin-1 Results in Embryonic Lethality and Severe Axon Guidance Defects without Increased Neural Cell Death. *Cell Rep* **12**, 1099-1106 (2015).
77. Arai, F. *et al.* Tie2/angiopoietin-1 signaling regulates hematopoietic stem cell quiescence in the bone marrow niche. *Cell* **118**, 149-161 (2004).
78. Walter, D. *et al.* Exit from dormancy provokes DNA-damage-induced attrition in haematopoietic stem cells. *Nature* **520**, 549-552 (2015).
79. Flach, J. *et al.* Replication stress is a potent driver of functional decline in ageing haematopoietic stem cells. *Nature* **512**, 198-202 (2014).
80. Ozmadenci, D. *et al.* Netrin-1 regulates somatic cell reprogramming and pluripotency maintenance. *Nat Commun* **6**, 7398 (2015).
81. Sung, P.J. *et al.* Cancer-Associated Fibroblasts Produce Netrin-1 to Control Cancer Cell Plasticity. *Cancer Res* **79**, 3651-3661 (2019).

82. Stein, S.J. & Baldwin, A.S. Deletion of the NF-kappaB subunit p65/RelA in the hematopoietic compartment leads to defects in hematopoietic stem cell function. *Blood* **121**, 5015-5024 (2013).
83. Asada, N. *et al.* Differential cytokine contributions of perivascular haematopoietic stem cell niches. *Nat Cell Biol* **19**, 214-223 (2017).
84. Baccin, C. *et al.* Combined single-cell and spatial transcriptomics reveals the molecular, cellular and spatial bone marrow niche organization. *bioRxiv* (2019).
85. Ding, L., Saunders, T.L., Enikolopov, G. & Morrison, S.J. Endothelial and perivascular cells maintain haematopoietic stem cells. *Nature* **481**, 457-462 (2012).
86. Kunisaki, Y. *et al.* Arteriolar niches maintain haematopoietic stem cell quiescence. *Nature* **502**, 637-643 (2013).

Figure legends

Figure 1: Neo1 is specifically expressed HSC and associated with quiescence.

a) Overview of hematopoietic stem and progenitor cells (HSPCs) and their immunophenotypes.

b) Relative expression of *Neo1* in HSPCs from 3 months old mice; n = 4-7 (HSC-MPPs), 9(CMP/MEP/GMP), 2 independent experiments.

c) MFI of NEO1 in HSPCs from 3 months old mice; n = 90 (MPP2), 118 (MPP34), 126 (MPP1), 145 (HSC), 2 independent experiments.

d) Relative expression of *Neo1* in dHSC and aHSC from *SCL-tTA; H2B-GFP* mice, chase for 5 months; n = 3.

e) MFI of NEO1 in dHSCs and aHSCs from *SCL-tTA; H2B-GFP* mice, chase for 5 months; n = 30 (aHSC) – 47 (dHSC).

f) Relative expression of *Neo1* in HSCs, 16 hours, 5 and 7 days after PBS or Poly-I:C injections; n = 3-5 (PBS16h).

g) Relative expression of *Neo1* in HSCs, 16 hours after PBS or LPS injections; n = 3 (LPS)-5 (PBS).

For all panels, ± SD is shown. N indicates biological replicates. Scale bars in IF images are 5 µm. P-value determined by two-tailed t test. Source data are provided as a Source Data file.

Figure 2: Mutant *Neo1* causes an initial HSC expansion

a) Relative expression of *Neo1* in total bone marrow of Wt and *Neo1*$^{gt/gt}$ mice; n = 6, 3 independent experiments.

b) Workflow: Generation of full chimeras.

c) Absolute frequencies of bone marrow CD45.2^{+} HSCs in full Wt and *Neo1*$^{gt/gt}$ chimeras 4 months after 1st and 2nd transplantation; n = 5 (2ndTx) – 8 (Ctrl 1st Tx), 9 (Neo1 1st TX), 2 independent experiments.

d) Workflow: Competitive transplantations.

e) Peripheral blood CD45.2^{+} chimerism during 1^{ary} and 2^{ary} competitive transplantations of Wt and *Neo1*$^{gt/gt}$ bone marrow; n = 13-17 (for exact n/timepoint please see Source data file), 3 independent experiments, Analysis with two-way-ANOVA, multiple comparison with LSD Fisher test.

f) CD45.2^{+} chimerism of HSCs at endpoints of 1^{ary} and 2^{ary} competitive transplantations of Wt and *Neo1* $^{gt//gt}$ bone marrow; n = 11 (2nd TX), 12 (Ctrl 1st Tx), 14(Neo1 1st TX), 3 independent experiments. Whiskers are Min-Max, Box is 25th-75th percentile, line is Mean.

g) Workflow: Full chimeras studied in h.

h) Absolute frequencies of bone marrow CD45.2^{+} HSCs in full Wt and *Neo1* $^{gt//gt}$ chimeras after 8 months; n = 8 (Ctrl) - 9 (Neo1), 2 independent experiments.

i) Workflow: Homing assay in j.

j) Absolute frequencies of CD45.2^{+} bone marrow LSK cells 48h after transplantation of 10.000 sorted Wt and *Neo1* $^{gt//gt}$ LSK; n = 5 (Ctrl) – 6 (Neo1).

For all panels, ± SD is shown. n indicates biological replicates. P-value determined by two-tailed t test unless stated otherwise. Source data are provided as a Source Data file.

Figure 3: Mutant *Neo1* causes premature HSC exhaustion

a) Workflow: Aged chimeras, analysed in b-d.

b) Absolute frequencies of bone marrow CD45.2$^+$ HSPCs in full Wt and *Neo1*$^{gt//gt}$ chimeras after 15 months; n = 7 (Ctrl) – 11(Neo1); 2 independent experiments.

c) Absolute blood counts of full Wt and *Neo1*$^{gt//gt}$ chimeras after 15 months; n = 7 (Ctrl) – 11 (Neo1), 2 independent experiments, for HB: 4 (Ctrl)- 7 (Neo1).

d) Frequencies of B- and myeloid cells of C45.2$^+$ cells in peripheral blood of Wt and *Neo1* $^{gt//gt}$ chimeras after 15 months; n = 5-13 (for exact n/timepoint please see Source data file), 2 independent experiments. Analysis with two-way-ANOVA, multiple comparisons with LSD Fisher test.

e) Workflow: Assessment of HSC potency derived from 15 months (aged) chimeras

f) Frequency of CD45.2$^+$ vs competitor HSCs 16 weeks transplantation of 100 or 500 HSCs from of aged Wt and *Neo1* $^{gt//gt}$ chimeras at; n = 6(Ctrl+ 500 HSC Neo1) - 7(100 HSC, Neo1), 2 independent experiments.

g) Workflow: Secondary and tertiary transplantations of 15 months (aged) chimeras.

h) Absolute frequencies of bone marrow CD45.2$^+$ HSPCs in 2^{ary} transplantations of aged Wt and *Neo1* $^{gt//gt}$ chimeras after 4 months; n = 7(Ctrl) -8 (Neo1), 2 independent experiments.

i) Absolute frequencies of bone marrow CD45.2$^+$ HSPCs in 3^{ary} transplantations of aged Wt and *Neo1* $^{gt//gt}$ chimeras after 4 months; n = 6, 2 independent experiments.

j) Workflow: Generating of full chimeras used in k-m.

k) Cell cycle phase of CD45.2$^+$ HSCs derived from Wt and *Neo1* $^{gt//gt}$ chimeras after 4 months; n = 4 (Ctrl) – 6 (Neo1), 2 independent experiments.

l) MFI of CDK6 in CD45.2$^+$ HSC derived from Wt and *Neo1* $^{gt//gt}$ chimeras after 4 months; n = 23 (Neo1) – 29 (Ctrl).

m) Frequency of BrdU$^+$ CD45.2$^+$ HSC derived from Wt and *Neo1* $^{gt//gt}$ chimeras after 4 months, 48 hours post BrdU injection; n = 6, 2 independent experiments.

For all panels, ± SD is shown. n indicates biological replicates. P-value determined by two-tailed t test unless stated otherwise. Source data are provided as a Source Data file.

Figure 4: *Neo1*-mutant HSCs reveal a loss of quiescence and potency signatures

a) Left: Workflow for RNA-seq of CD45.2^{+} HSCs from Wt and *Neo1* $^{gt//gt}$ chimeras after 4 and 15 months, Right: Sparce-PCA; n = 2 (WT old/ young, Neo1 young) - 3 (Neo1 old).

b) GSEA for cell cycle and HSC potency of Wt *vs*. *Neo1* $^{gt//gt}$ HSCs. FDR < 0.05, NOM p-value < 0.05.

c) Normalised read counts of DEG in HSCs from young and old Wt and *Neo1* $^{gt//gt}$ chimeras, n = 4 (Ctrl) - 5 (Neo1).

d) GSEA for HSC ageing signatures in Wt *vs. Neo1* $^{gt//gt}$ HSCs. FDR < 0.05, NOM p-value < 0.05.

e) Normalised read counts of *Klf6* in HSCs from young and old Wt and *Neo1* $^{gt//gt}$ chimeras, n = 4 (Ctrl)-5 (Neo1).

f) GSEA for signalling pathways in Wt *vs*. *Neo1* $^{gt//gt}$ HSCs. FDR < 0.05, NOM p-value < 0.05.

For all panels, ± SD is shown. n indicates biological replicates. Scale bars in IF images are 4µm. P-value determined by two-tailed t test unless stated otherwise. Source data are provided as a Source Data file.

Figure 5: Ntn1 preserves HSC quiescence and engraftment potential *in vitro via* Neo1

a) Workflow: *In vitro* stimulation of sorted HSCs used in b-d, analysis after 48 h.

b) Relative expression of *Egr1* in Wt HSCs; n = 3(other), 4 (RGMa+b), 16 (Ctrl/Neo1), for ctrl / Ntn1, 4 independent experiments.

c) Representative cell cycle plots pre-gated on HSCs and quantification with or without Ntn1 treatment; n = 3 (Neo1),11 (Wt- Ctrl),12 (Wt-Ntn1), 3 independent experiments for ctrl HSC.

d) MFI of CDK6 in Wt HSCs 48 h after Ntn1 treatment, quantification of MFI per cell; n = 114 (Ctrl), 134 (Ntn1).

e) Workflow: representative images and quantification of total cell / nuclear MFI of p65-GFP HSC 48 h after treatment with Ntn1 or Ntn1+JSH-23; n = 8 (JSH-23), 78 (Ctrl), 91 (Ntn1), 2 independent experiments.

f) Workflow: Competitive transplantation of Ntn1 stimulated CD45.2 and CD45.1/2 HSCs.

g) Chimerism of bone marrow LSK-SLAM cells 4 months after competitive transplantation of Control- versus Ntn1 treated HSCs; n = 6 (CD45.1/2), 7 (CD45.2); 2 independent experiments.

For all panels, ± SD is shown. n indicates biological replicates. Scale bars in IF images are 4 µm. P-value determined by two-tailed t test unless stated otherwise. Source data are provided as a Source Data file.

Figure 6: *In vivo Ntn1* deletion depletes HSC and Ntn1 overexpression increases HSC quiescence

a) Workflow: Analysis of *Ntn1*$^{flox/flox}$ and *CAGGS:Cre*^{ERT2}*; Ntn1*$^{flox/flox}$ mice 8 weeks after Cre induction for b-e.

b) Representative flow cytometry plots of the LSK population of *Ntn1*$^{flox/flox}$ and *Ntn1*$^{\Delta CAGGS/\Delta CAGGS}$ mice.

c) Frequencies of bone marrow HSCs in *Ntn1*$^{flox/flox}$ and *Ntn1*$^{\Delta CAGGS/\Delta CAGGS}$ mice; n = 7(flox)-10 (ΔCAGGS), 2 independent experiments.

d) Cell cycle phase of HSCs derived from *Ntn1*$^{flox/flox}$ and *Ntn1*$^{\Delta CAGGS/\Delta CAGGS}$ mice; n = 8 (flox), 10 (ΔCAGGS), 2 independent experiments.

e) Relative expression of quiescence and activation related genes in HSCs derived from *Ntn1*$^{flox/flox}$ and *Ntn1*$^{\Delta CAGGS/\Delta CAGGS}$ mice; n = 6 (flox) - 9 (ΔCAGGS), 2 independent experiments.

f) Frequencies of bone marrow HSCs in *Ntn1*$^{flox/flox}$ and *Ntn1*$^{\Delta CAGGS/\Delta CAGGS}$ mice 5 months after Cre induction; n = 8 (ΔCAGGS), 12 (flox), 3 independent experiments.

g) Cell cycle phase of HSCs derived from *Ntn1*$^{+/LSL\text{-}Rosa26\text{-}Ntn1}$ and *Ntn1-OE* mice; n = 8 (ΔCAGGS), 12 (flox), 3 independent experiments.

h) Workflow: Competitive transplantation of *CAGGS:Cre*^{ERT2}, *Ntn1*$^{\Delta CAGGS/\Delta CAGGS}$ and Ntn1-OE mice 5 months after Cre induction, analysed in i-k

i) Representative FACS plots of eripheral blood leukocytes pregated on CD45+ cells at 16 weeks after transplantation.

j) Peripheral blood CD45.2^{+} chimerism during competitive transplantations; n = 13 (OE)-14(Cre/ ΔCAGGS), two independent experiments, Analysis with two-way-ANOVA, multiple comparison with LSD Fisher test.

k) Bone marrow HSC CD45.2^{+} chimerism after 16 weeks of competitive transplantation n = 12 (Cre) – 13 (ΔCAGGS/ OE) , 2independent experiments.

l) Workflow: Transplantation of 200 HSCs sorted from *CAGGS:Cre*^{ERT2} and *Ntn1*$^{\Delta CAGGS/\Delta CAGGS}$ mice at 5 months after Cre induction.

m) Frequencies of bone marrow HSCs 8 weeks transplantation; n = 6.

For all panels, ± SD is shown. n indicates biological replicates. P-value determined by two-tailed t test unless stated otherwise. Source data are provided as a Source Data file.

Figure 7: Loss of niche derived Ntn1 induces Neo1 in HSC upon ageing

a) Relative expression of *Ntn1* in $CD45^+$ and niche populations derived from *Sma-RFP* mice; n = 4 (CD45/AEC), 6 (SEC), 7 (SMA-RFP), 2 independent experiments.

b) Frequencies of HSCs in bone marrow of in $Ntn1^{flox/flox}$ and $Ntn1^{\Delta Sma/\Delta Sma}$ mice; n = 8 (flox), 10 (ΔSMA), 3 independent experiments.

c) Relative expression of *Ntn1* in endothelial and $CD45^+$ cells derived from young and old Wt mice; n = 3 (yCD45/oAEC), 4 (oSEC), 6 (ySEC), 7 (yAEC), 3 independent experiments.

d) Normalised read counts of *Neo1* in young, and old LSK-SLAM cells, n = 5 (young), 7 (old) FDR < 0.0001.

e) MFI of NEO1 in sorted 6 or 24 months LSK-SLAM cells; n = 592 (young) - 593 (old).

f) Most abundant common DEGs in published aging studies and own data, additional details in M&M section.

g) Relative expression of *Neo1* in LSK-SLAM cells isolated from either denervated or healthy legs of individual mice; n = 8, 2 independent experiments.

h) Relative expression of *Neo1* in HSCs of aged mice, before and after 2 months post transplantation; n = 6 (before), 8 (after), 2 independent experiments.

i) Model of Neo1 / Ntn1 axis in young and old mice.

For all panels, ± SD is shown. n indicates biological replicates. Scale bars in IF images are 5 µm. P-value determined by two-tailed t test unless stated otherwise. Source data are provided as a Source Data file.

Figure 1

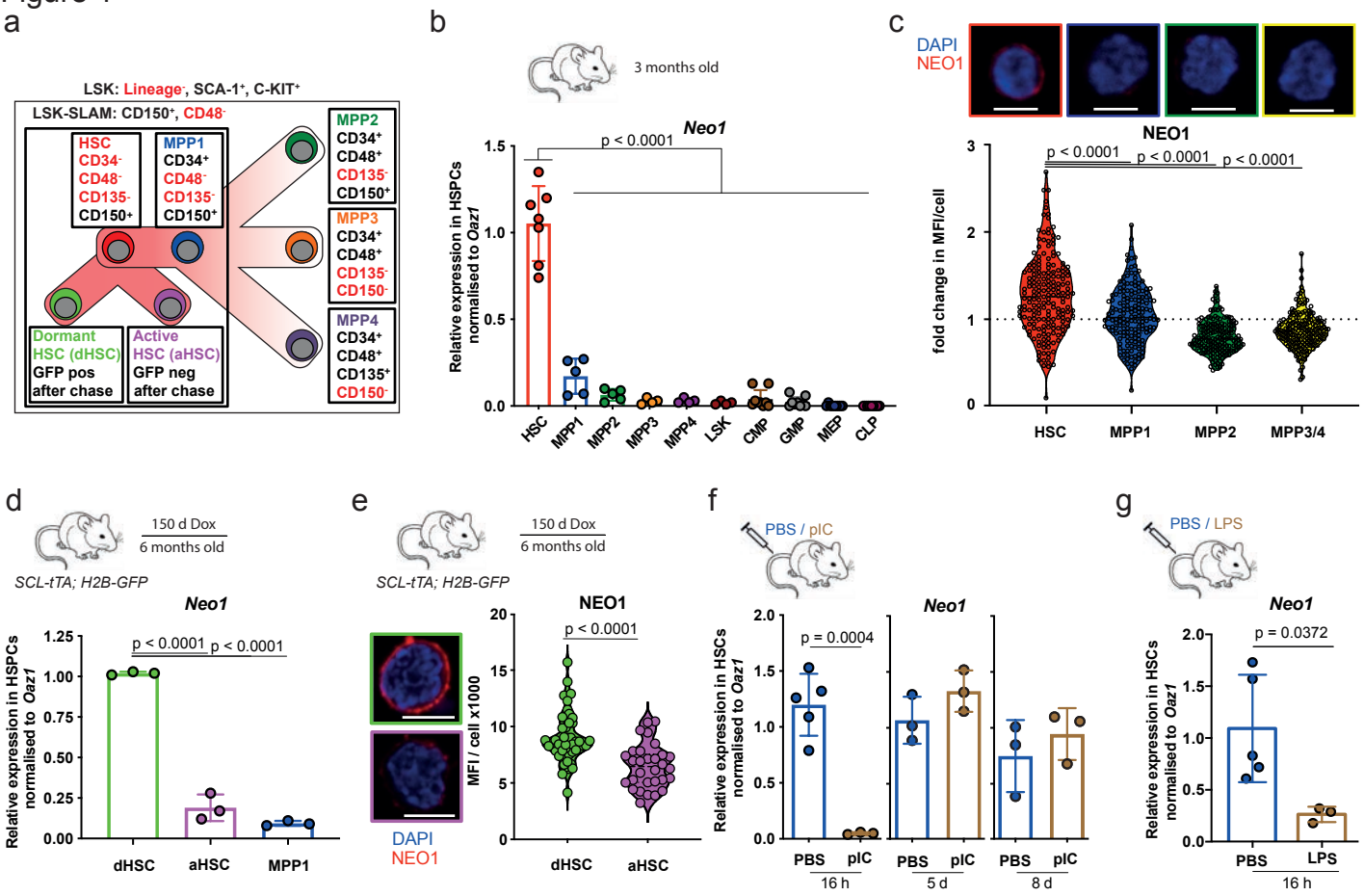
a
LSK: Lineage-, SCA-1+, C-KIT+
LSK-SLAM: CD150+, CD48-
HSC CD34- CD48- CD135- CD150+
MPP1 CD34+ CD48- CD135- CD150+
MPP2 CD34+ CD48+ CD135- CD150+
MPP3 CD34+ CD48+ CD135- CD150-
MPP4 CD34+ CD48+ CD135+ CD150-
Dormant HSC (dHSC) GFP pos after chase
Active HSC (aHSC) GFP neg after chase
b
3 months old
Neo1
p < 0.0001
Relative expression in HSPCs normalised to Oaz1
HSC MPP1 MPP2 MPP3 MPP4 LSK CMP GMP MEP CLP
c
DAPI
NEO1
NEO1
p < 0.0001 p < 0.0001 p < 0.0001
fold change in MFI/cell
HSC MPP1 MPP2 MPP3/4
d
150 d Dox
6 months old
SCL-tTA; H2B-GFP
Neo1
p < 0.0001 p < 0.0001
Relative expression in HSPCs normalised to Oaz1
dHSC aHSC MPP1
e
150 d Dox
6 months old
SCL-tTA; H2B-GFP
DAPI
NEO1
NEO1
p < 0.0001
MFI / cell x1000
dHSC aHSC
f
PBS / pIC
Neo1
p = 0.0004
Relative expression in HSCs normalised to Oaz1
PBS pIC
16 h
PBS pIC
5 d
PBS pIC
8 d
g
PBS / LPS
Neo1
p = 0.0372
Relative expression in HSCs normalised to Oaz1
PBS LPS
16 h

Figure 2

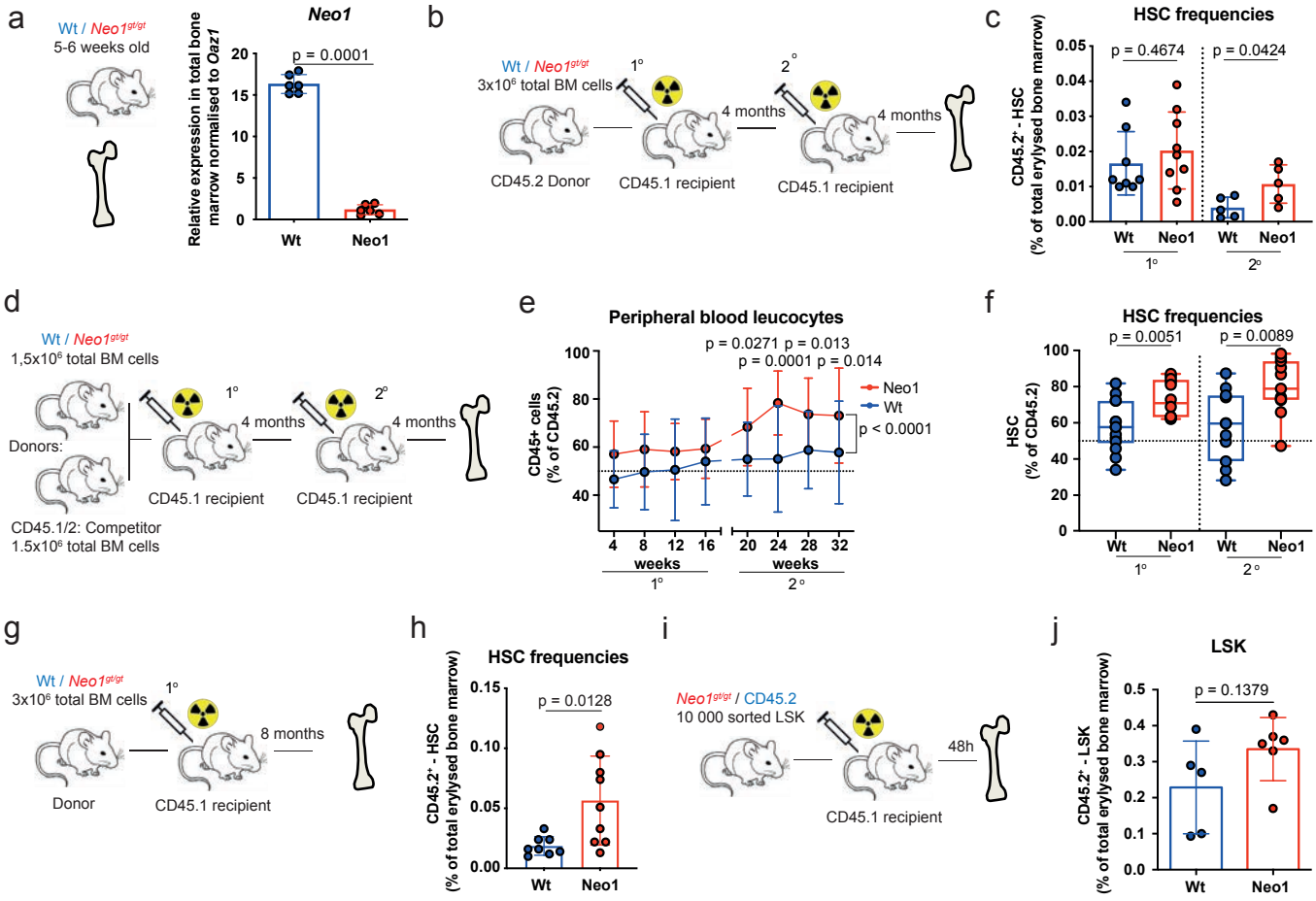
a
Wt / Neo1gt/gt
5-6 weeks old
Neo1
p = 0.0001
Relative expression in total bone marrow normalised to Oaz1
Wt
Neo1
b
Wt / Neo1gt/gt
3x10⁶ total BM cells
1°
2°
4 months
4 months
CD45.2 Donor
CD45.1 recipient
CD45.1 recipient
c
HSC frequencies
p = 0.4674
p = 0.0424
CD45.2+ - HSC (% of total erylysed bone marrow)
Wt
Neo1
Wt
Neo1
1°
2°
d
Wt / Neo1gt/gt
1,5x10⁶ total BM cells
Donors:
1°
2°
4 months
4 months
CD45.1 recipient
CD45.1 recipient
CD45.1/2: Competitor
1.5x10⁶ total BM cells
e
Peripheral blood leucocytes
p = 0.0271 p = 0.013
p = 0.0001 p = 0.014
Neo1
Wt
p < 0.0001
CD45+ cells (% of CD45.2)
weeks
weeks
1°
2°
f
HSC frequencies
p = 0.0051
p = 0.0089
HSC (% of CD45.2)
Wt
Neo1
Wt
Neo1
1°
2°
g
Wt / Neo1gt/gt
3x10⁶ total BM cells
1°
8 months
Donor
CD45.1 recipient
h
HSC frequencies
p = 0.0128
CD45.2+ - HSC (% of total erylysed bone marrow)
Wt
Neo1
i
Neo1gt/gt / CD45.2
10 000 sorted LSK
48h
CD45.1 recipient
j
LSK
p = 0.1379
CD45.2+ - LSK (% of total erylysed bone marrow)
Wt
Neo1

Figure 3

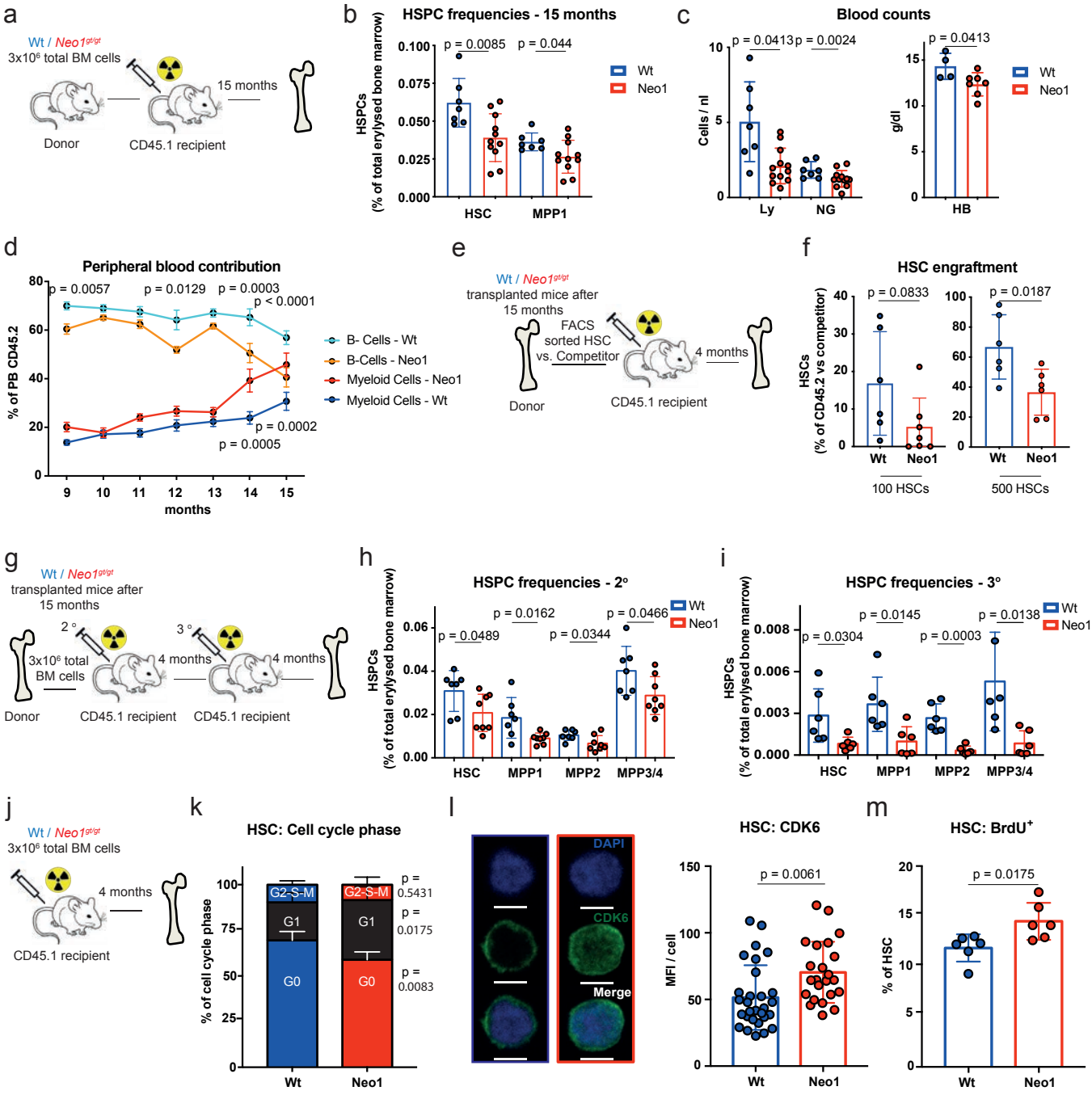
a
Wt / Neo1gt/gt
3x10⁶ total BM cells
15 months
Donor
CD45.1 recipient
b
HSPC frequencies - 15 months
HSPCs (% of total erylysed bone marrow)
p = 0.0085
p = 0.044
Wt
Neo1
HSC
MPP1
c
Blood counts
p = 0.0413
p = 0.0024
Cells / nl
Ly
NG
p = 0.0413
g/dl
HB
d
Peripheral blood contribution
% of PB CD45.2
p = 0.0057
p = 0.0129
p = 0.0003
p < 0.0001
p = 0.0002
p = 0.0005
B- Cells - Wt
B-Cells - Neo1
Myeloid Cells - Neo1
Myeloid Cells - Wt
months
e
Wt / Neo1gt/gt
transplanted mice after
15 months
FACS
sorted HSC
vs. Competitor
4 months
Donor
CD45.1 recipient
f
HSC engraftment
HSCs (% of CD45.2 vs competitor)
p = 0.0833
p = 0.0187
Wt
Neo1
100 HSCs
500 HSCs
g
Wt / Neo1gt/gt
transplanted mice after
15 months
2 °
3 °
3x10⁶ total
BM cells
4 months
4 months
Donor
CD45.1 recipient
CD45.1 recipient
h
HSPC frequencies - 2°
HSPCs (% of total erylysed bone marrow)
p = 0.0489
p = 0.0162
p = 0.0344
p = 0.0466
Wt
Neo1
HSC
MPP1
MPP2
MPP3/4
i
HSPC frequencies - 3°
HSPCs (% of total erylysed bone marrow)
p = 0.0304
p = 0.0145
p = 0.0003
p = 0.0138
Wt
Neo1
HSC
MPP1
MPP2
MPP3/4
j
Wt / Neo1gt/gt
3x10⁶ total BM cells
4 months
CD45.1 recipient
k
HSC: Cell cycle phase
% of cell cycle phase
G2-S-M
G1
G0
p = 0.5431
p = 0.0175
p = 0.0083
Wt
Neo1
l
DAPI
CDK6
Merge
m
HSC: CDK6
MFI / cell
p = 0.0061
Wt
Neo1
HSC: BrdU+
% of HSC
p = 0.0175
Wt
Neo1

Figure 4

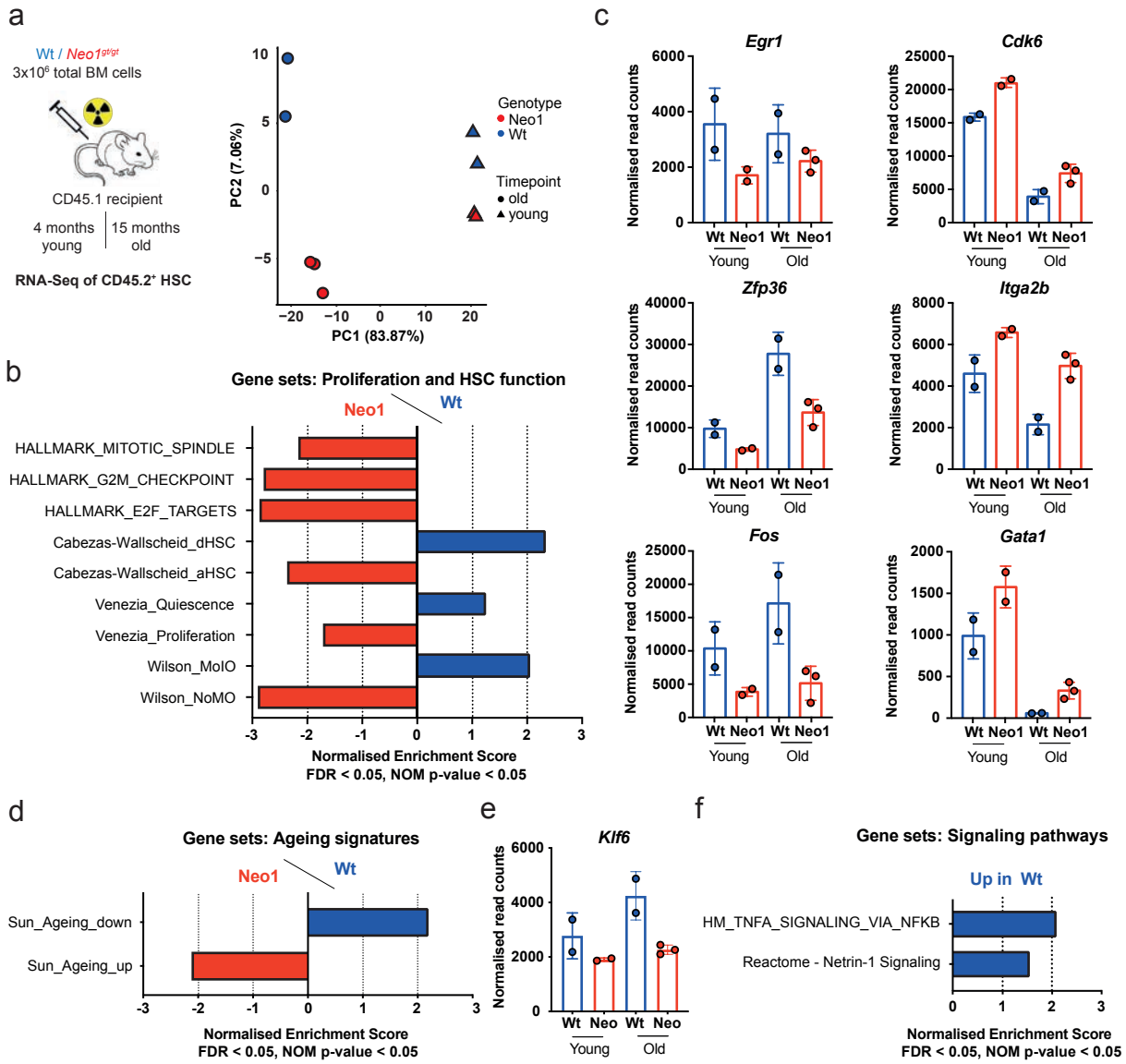
a
Wt / Neo1gt/gt
3x10⁶ total BM cells
CD45.1 recipient
4 months young
15 months old
RNA-Seq of CD45.2+ HSC
PC2 (7.06%)
PC1 (83.87%)
Genotype
Neo1
Wt
Timepoint
old
young
b
Gene sets: Proliferation and HSC function
Neo1
Wt
HALLMARK_MITOTIC_SPINDLE
HALLMARK_G2M_CHECKPOINT
HALLMARK_E2F_TARGETS
Cabezas-Wallscheid_dHSC
Cabezas-Wallscheid_aHSC
Venezia_Quiescence
Venezia_Proliferation
Wilson_MoIO
Wilson_NoMO
Normalised Enrichment Score
FDR < 0.05, NOM p-value < 0.05
c
Egr1
Cdk6
Zfp36
Itga2b
Fos
Gata1
Normalised read counts
Wt Neo1 Wt Neo1
Young
Old
d
Gene sets: Ageing signatures
Neo1
Wt
Sun_Ageing_down
Sun_Ageing_up
Normalised Enrichment Score
FDR < 0.05, NOM p-value < 0.05
e
Klf6
Normalised read counts
Wt Neo Wt Neo
Young
Old
f
Gene sets: Signaling pathways
Up in Wt
HM_TNFA_SIGNALING_VIA_NFKB
Reactome - Netrin-1 Signaling
Normalised Enrichment Score
FDR < 0.05, NOM p-value < 0.05

Figure 5

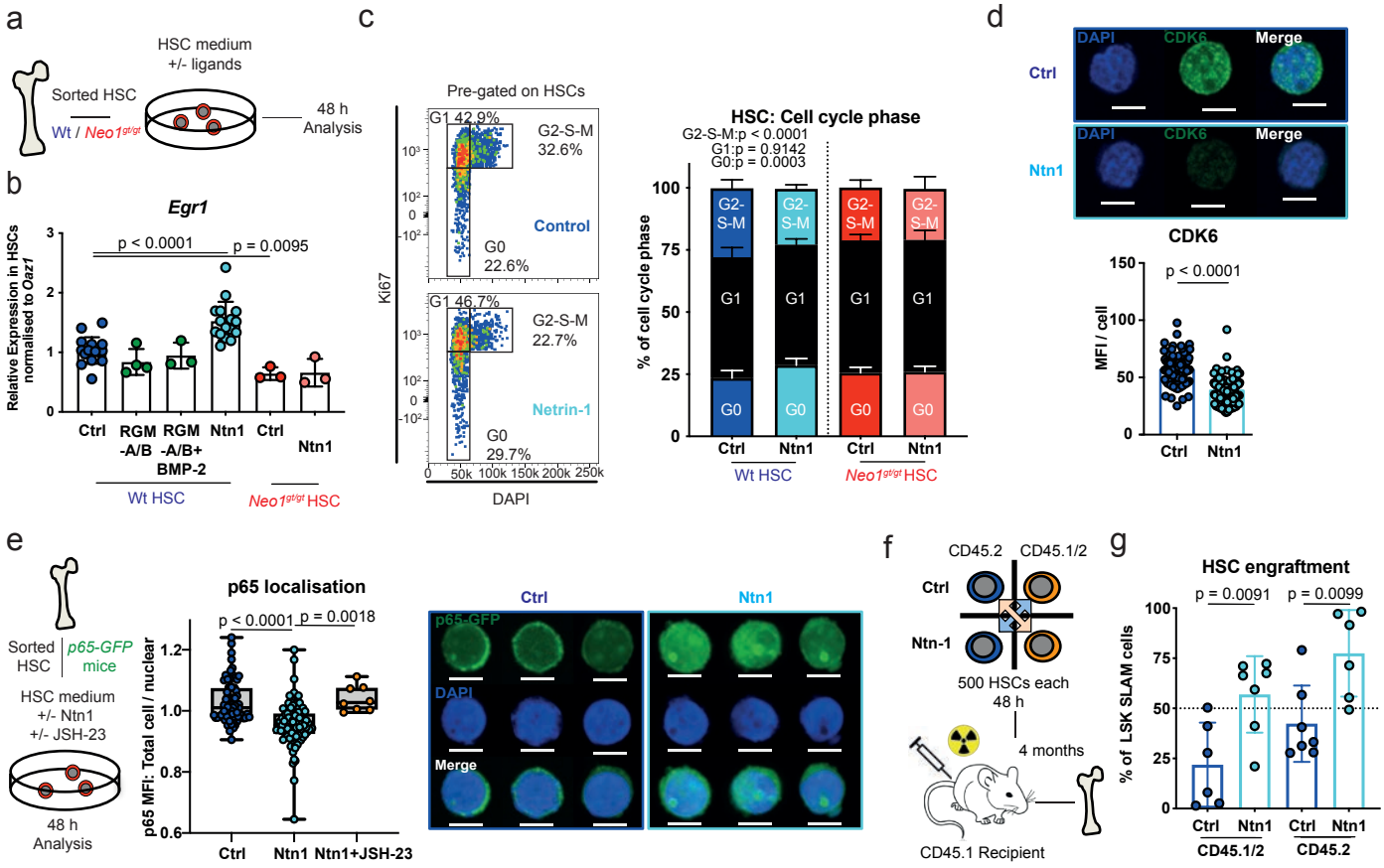
a
HSC medium
+/- ligands
Sorted HSC
Wt / Neo1gt/gt
48 h
Analysis
b
Egr1
p < 0.0001
p = 0.0095
Relative Expression in HSCs normalised to Oaz1
Ctrl
RGM -A/B
RGM -A/B+ BMP-2
Ntn1
Ctrl
Ntn1
Wt HSC
Neo1gt/gt HSC
c
Pre-gated on HSCs
G1 42.9%
G2-S-M 32.6%
Control
G0 22.6%
G1 46.7%
G2-S-M 22.7%
Netrin-1
G0 29.7%
Ki67
DAPI
HSC: Cell cycle phase
G2-S-M:p < 0.0001
G1:p = 0.9142
G0:p = 0.0003
% of cell cycle phase
G2-S-M
G1
G0
Ctrl
Ntn1
Wt HSC
Neo1gt/gt HSC
d
DAPI
CDK6
Merge
Ctrl
Ntn1
CDK6
p < 0.0001
MFI / cell
e
Sorted HSC
p65-GFP mice
HSC medium
+/- Ntn1
+/- JSH-23
48 h
Analysis
p65 localisation
p < 0.0001
p = 0.0018
p65 MFI: Total cell / nuclear
Ctrl
Ntn1
Ntn1+JSH-23
p65-GFP
DAPI
Merge
f
CD45.2
CD45.1/2
Ctrl
Ntn-1
500 HSCs each
48 h
4 months
CD45.1 Recipient
g
HSC engraftment
p = 0.0091
p = 0.0099
% of LSK SLAM cells
Ctrl
Ntn1
CD45.1/2
CD45.2

Figure 6

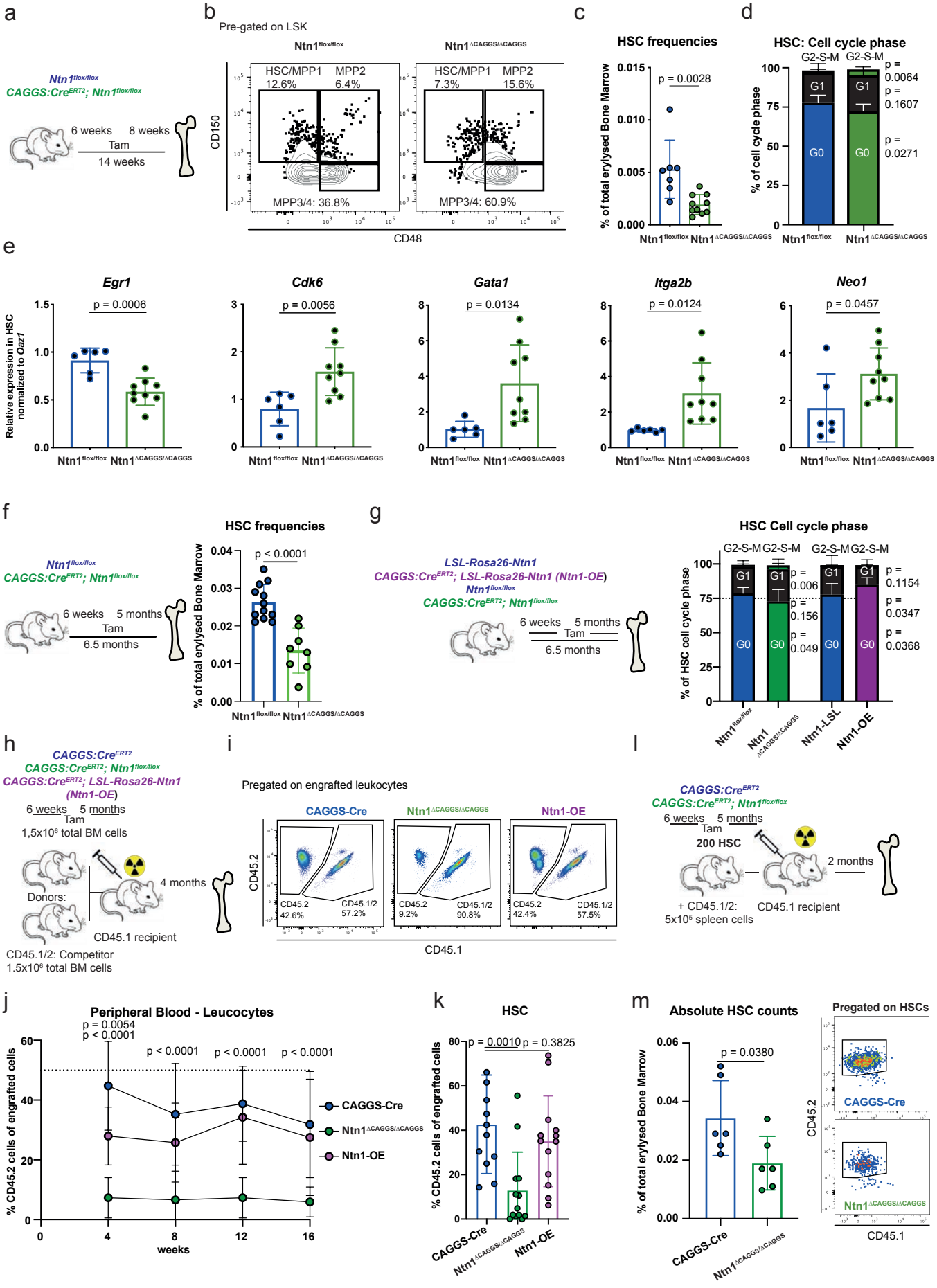
a
Ntn1flox/flox
CAGGS:CreERT2; Ntn1flox/flox
6 weeks
8 weeks
Tam
14 weeks
b
Pre-gated on LSK
Ntn1flox/flox
Ntn1ΔCAGGS/ΔCAGGS
HSC/MPP1 12.6%
MPP2 6.4%
MPP3/4: 36.8%
HSC/MPP1 7.3%
MPP2 15.6%
MPP3/4: 60.9%
CD150
CD48
c
HSC frequencies
p = 0.0028
% of total erylysed Bone Marrow
d
HSC: Cell cycle phase
G2-S-M
G1
G0
p = 0.0064
p = 0.1607
p = 0.0271
% of cell cycle phase
e
Egr1
p = 0.0006
Cdk6
p = 0.0056
Gata1
p = 0.0134
Itga2b
p = 0.0124
Neo1
p = 0.0457
Relative expression in HSC normalized to Oaz1
f
HSC frequencies
Ntn1flox/flox
CAGGS:CreERT2; Ntn1flox/flox
6 weeks
5 months
Tam
6.5 months
p < 0.0001
% of total erylysed Bone Marrow
g
HSC Cell cycle phase
LSL-Rosa26-Ntn1
CAGGS:CreERT2; LSL-Rosa26-Ntn1 (Ntn1-OE)
Ntn1flox/flox
CAGGS:CreERT2; Ntn1flox/flox
6 weeks
5 months
Tam
6.5 months
p = 0.006
p = 0.156
p = 0.049
p = 0.1154
p = 0.0347
p = 0.0368
% of HSC cell cycle phase
Ntn1-LSL
Ntn1-OE
h
CAGGS:CreERT2
CAGGS:CreERT2; Ntn1flox/flox
CAGGS:CreERT2; LSL-Rosa26-Ntn1 (Ntn1-OE)
6 weeks
5 months
Tam
1,5x10⁶ total BM cells
Donors:
4 months
CD45.1 recipient
CD45.1/2: Competitor
1.5x10⁶ total BM cells
i
Pregated on engrafted leukocytes
CAGGS-Cre
Ntn1ΔCAGGS/ΔCAGGS
Ntn1-OE
CD45.2
CD45.1
CD45.2 42.6%
CD45.1/2 57.2%
CD45.2 9.2%
CD45.1/2 90.8%
CD45.2 42.4%
CD45.1/2 57.5%
l
CAGGS:CreERT2
CAGGS:CreERT2; Ntn1flox/flox
6 weeks
5 months
Tam
200 HSC
2 months
+ CD45.1/2:
5x10⁵ spleen cells
CD45.1 recipient
j
Peripheral Blood - Leucocytes
p = 0.0054
p < 0.0001
p < 0.0001
p < 0.0001
p < 0.0001
% CD45.2 cells of engrafted cells
weeks
CAGGS-Cre
Ntn1ΔCAGGS/ΔCAGGS
Ntn1-OE
k
HSC
p = 0.0010
p = 0.3825
% CD45.2 cells of engrafted cells
m
Absolute HSC counts
p = 0.0380
% of total erylysed Bone Marrow
Pregated on HSCs
CAGGS-Cre
Ntn1ΔCAGGS/ΔCAGGS
CD45.2
CD45.1

Figure 7

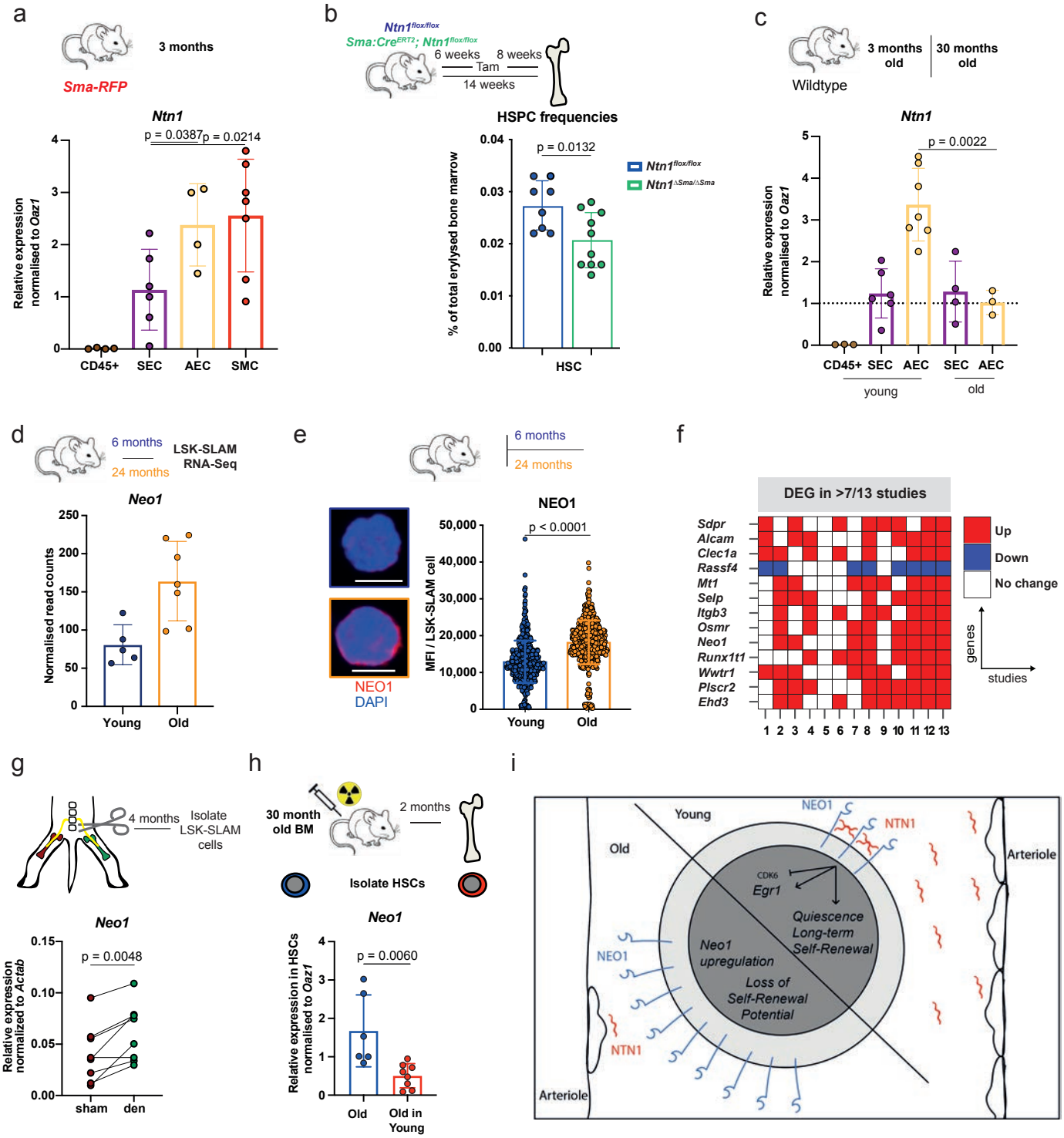
a
3 months
Sma-RFP
Ntn1
p = 0.0387
p = 0.0214
Relative expression normalised to Oaz1
CD45+
SEC
AEC
SMC
b
Ntn1flox/flox
Sma:CreERT2; Ntn1flox/flox
6 weeks
8 weeks
Tam
14 weeks
HSPC frequencies
p = 0.0132
% of total erylysed bone marrow
Ntn1flox/flox
Ntn1ΔSma/ΔSma
HSC
c
3 months old
30 months old
Wildtype
Ntn1
p = 0.0022
Relative expression normalised to Oaz1
CD45+
SEC
AEC
SEC
AEC
young
old
d
6 months
24 months
LSK-SLAM RNA-Seq
Neo1
Normalised read counts
Young
Old
e
6 months
24 months
NEO1
DAPI
NEO1
p < 0.0001
MFI / LSK-SLAM cell
Young
Old
f
DEG in >7/13 studies
Sdpr
Alcam
Clec1a
Rassf4
Mt1
Selp
Itgb3
Osmr
Neo1
Runx1t1
Wwtr1
Plscr2
Ehd3
Up
Down
No change
genes
studies
1 2 3 4 5 6 7 8 9 10 11 12 13
g
4 months
Isolate LSK-SLAM cells
Neo1
p = 0.0048
Relative expression normalized to Actab
sham
den
h
30 month old BM
2 months
Isolate HSCs
Neo1
p = 0.0060
Relative expression in HSCs normalised to Oaz1
Old
Old in Young
i
Young
Old
NEO1
NTN1
Arteriole
CDK6
Egr1
Quiescence
Long-term
Self-Renewal
Neo1
upregulation
Loss of
Self-Renewal
Potential
NEO1
NTN1
Arteriole